STATIC TESTS OF 1/20-SCALE MODELS OF THE CLINCH RIVER BREEDER REACTOR HEAD IN SUPPORT ON THE LMFBR SAFETY PROGRAM

Final Report

December 1982

By: C. M. Romander and Y. D. Murray
A. L. Florence, Project Supervisor

Prepared for:

U.S. DEPARTMENT OF ENERGY
Safety Section
Headquarters
Germantown, MD

DOE Contract DE-AT03-82-SF11670

SRI Project PYU 4671

SRI International
333 Ravenswood Avenue
Menlo Park, California 94025
(415) 326-6200
TWX: 910-373-2046
Telex: 334 486

ABSTRACT

Two static tests of 1/20-scale models of the Clinch River Breeder Reactor (CRBR) head were performed to evaluate the effects of below-head shielding design and attachment on the strength of the head. The first static test (SM 7) was on the undamaged three-plug head and bolted shielding tested previously in dynamic test SM 4, which was designed to investigate the response of the CRBR to a 661 MW-s HCDA loading. Data from 17 displacement gages and 1 pressure gage on this head model were used in a single-degree-of-freedom (SDOF) dynamic response analysis to interpret the head deflection measured in dynamic test SM 5, which was a repeat test of SM 4. The second static test (SM 8) was on the undamaged head from test SM 5. The shielding was replaced by a set of more prototypical design and attached to the head in a more prototypical manner. Data from SM 8 were used in the SDOF analysis to predict the dynamic response of a head with prototypic shielding to the HCDA slug impact loading.

In both tests, the models were loaded to failure. For both, failure was caused by disengagement of the shear ring between the large rotating plug (LRP) and the intermediate rotating plug (IRP). Because of the asymmetry of the three-plug head, disengagement was a gradual process that began when the displacement of the head reached about 130 mils at the junction of the IRP and LRP nearest the center of the head. Failure was complete when the displacement at this location reached 250 mils (at a load of 2587 psi on SM 7 and 2010 psi on SM 8). Load-volume change records for each model show that the head with prototypic shielding (SM 8) has a stiffness in the linear-elastic range (below deflections of about 60 mils) that is 33% lower than the head with stiff, bolted shielding (SM 7).

Among the various models chosen for the SDOF analysis of the head with bolted shielding (SM 7), a reasonable one was used to calculate a

peak dynamic deflection of 89 mils compared with 60 mils measured in test SM 5. A similar model for the SDOF analysis of the head with prototypic shielding (SM 8) predicts a peak dynamic deflection of 110 mils.

The difference between the measured and calculated displacements for test SM 5 implies that a mechanism was acting in the dynamic experiment to limit head deflection. This mechanism is the interaction of the upper internal structure (UIS) with the IRP because the UIS is keyed into the core support structure and it cannot displace laterally. This interaction provides a substantial moment that resists IRP rotation and hence head deflection.

ACKNOWLEDGMENTS

The authors acknowledge L. E. Strawbridge, A. M. Christie, and M. A. Todd, of Westinghouse-Advanced Reactor Division (W-ARD), who provided technical guidance and the design drawings for the prototypic shielding tested on this program.

The technical staff of Poulter Laboratory at SRI International performed a wide variety of tasks to ensure the successful completion of the static tests. In particular, G. Greenfield supervised the fabrication of the shielding and test apparatus, A. Urweider, T. Lovelace, and E. Turner machined the parts needed for the shielding and test apparatus, K. Stepleton provided photographic and technical support, C. Benson assembled the models and conducted the tests, and E. Eckert and D. Walter provided the electronic support. B. Bain reduced the data. L. E. Schwer performed finite element analysis in support of the single-degree-of-freedom analysis. The help of these people is gratefully acknowledged.

CONTENTS

ILLUSTRATIONS

TABLES

I INTRODUCTION

A. Background

One of the important considerations in the safety analysis of the Clinch River Breeder Reactor (CRBR) is the ability of the three-plug head of the reactor (Figure 1) to remain tightly sealed after a hypothetical core disruptive accident (HCDA). During such an accident, it is possible for the sodium pool above the core to be driven upward to impact the head. Failure of the shear rings that restrain the plugs from upward motion or gross deformation of the head could provide leak paths for radioactive materials.

An experimental program was conducted at SRI International in 1977 to investigate the dynamic response of 1/20-scale models of the CRBR to simulated HCDAs.[1] During this experimental program, two tests (SM 4 and SM 5) were performed on complex models of the CRBR. These models included the vessel, core support structure, upper internal structure, and most important, the three-plug head with shear rings and below-head shielding (Figure 2). The results of these tests indicated that for a simulated 661 MW-s HCDA, the head would remain tightly sealed because all deformations in and around the head closure were elastic. The peak head displacement measured on test SM 5 was about 0.060 inch, well within the elastic limit of the head (0.080 inch) based on a static test (SM 1) performed on the three-plug head without shielding. In addition, a dynamic elastic analysis was performed on the head using an equivalent

---

[1] C. M. Romander and D. J. Cagliostro, "Structural Response of 1/20-Scale Models of the Clinch River Breeder Reactor to a Simulated Hypothetical Core Disruptive Accident," Technical Report 4 for the U.S. Department of Energy, Reactor Research and Technology, Contract No. EY-76-C-03-0115, SRI Project PYU-3929 (October 1978).

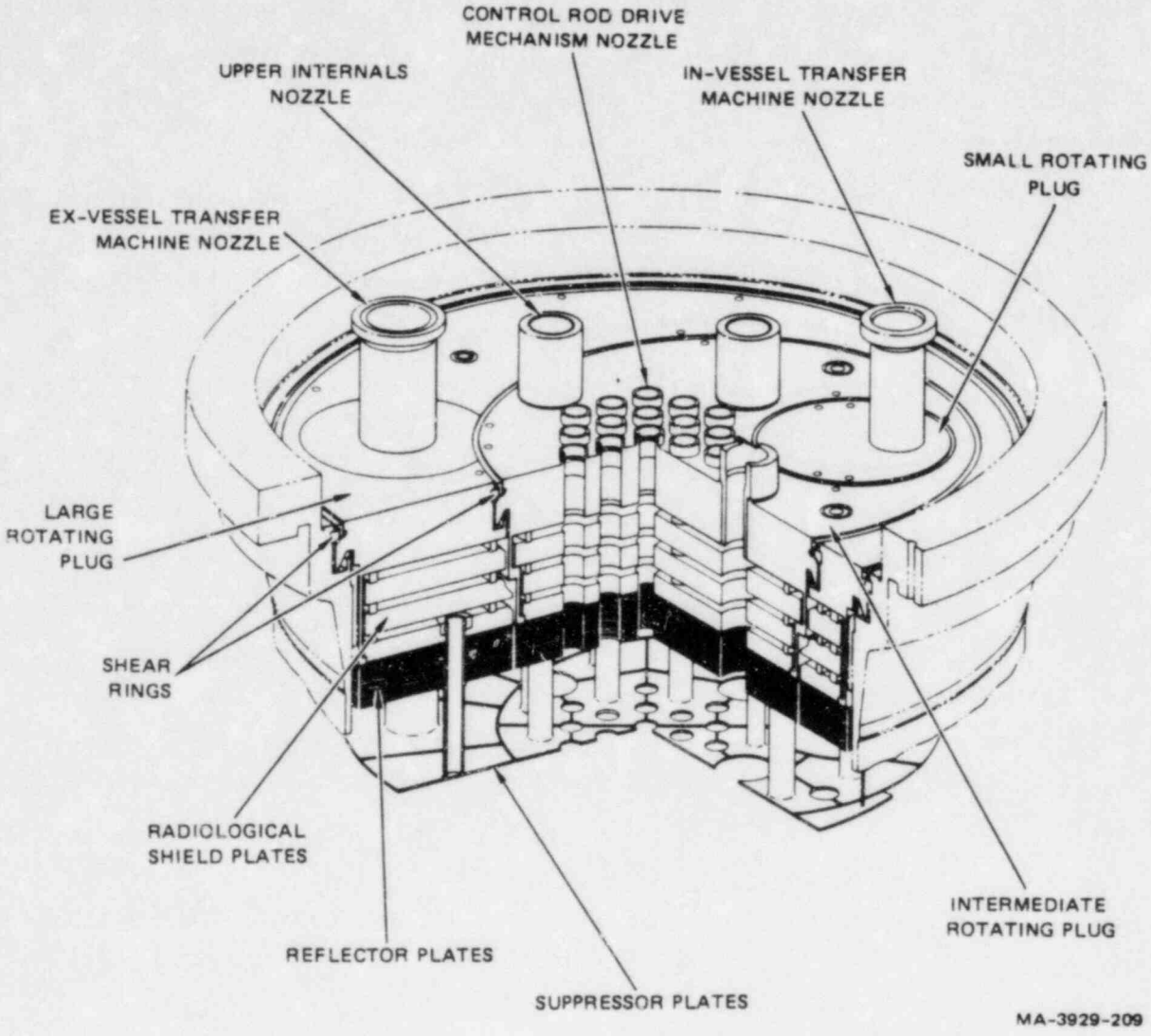

FIGURE 1 CRBR ROTATING PLUG HEAD DESIGN

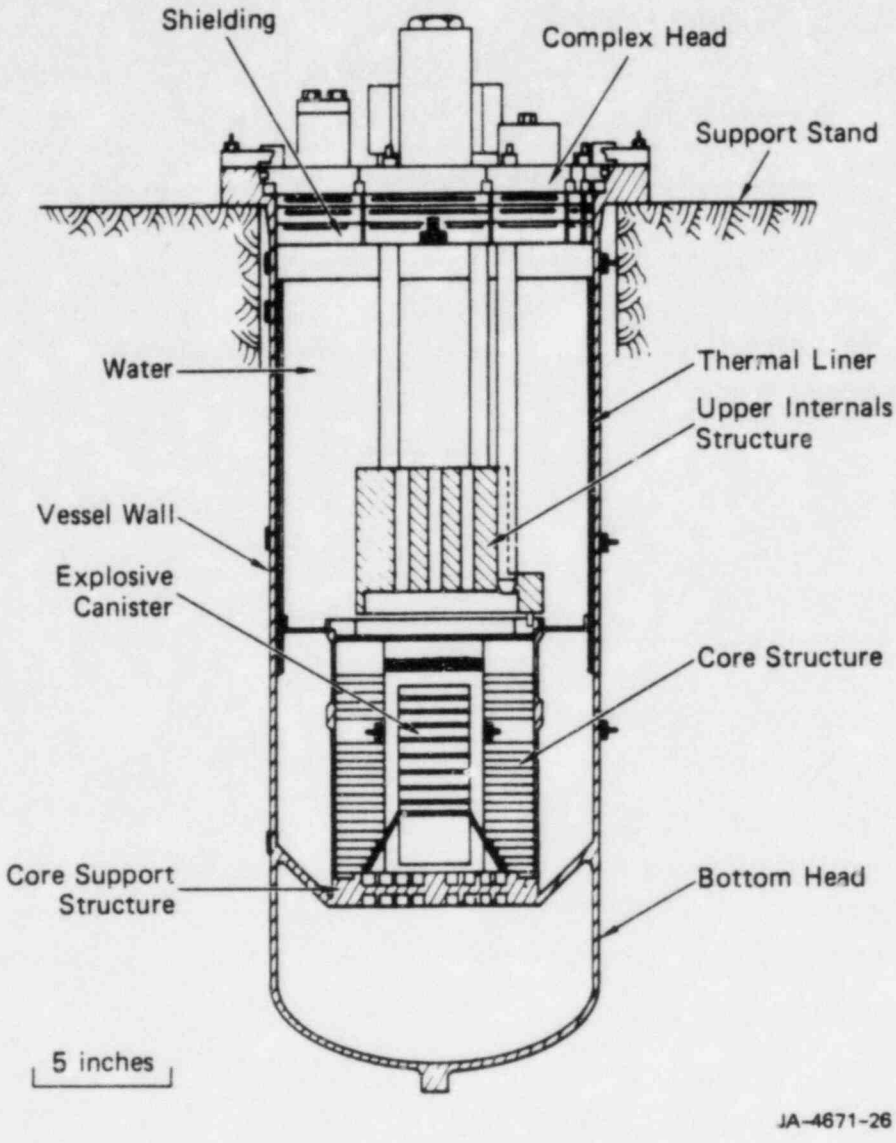

FIGURE 2 SCHEMATIC OF COMPLEX MODELS SM 4 AND SM 5

single-degree-of-freedom (SDOF) technique.[2] The head stiffness was approximated by adding the stiffnesses obtained in test SM 1 to theoretical approximations for the shielding plate stiffnesses. The analysis gave a maximum deflection of 0.129 inch.*

A recent review of this work by the Nuclear Regulatory Commission (NRC) resulted in some questions about the results of these dynamic tests. These questions centered on the modeling of the head and attached shielding in tests SM 4 and SM 5 and on the methods used to derive the head stiffness for the SDOF analysis. In particular, the NRC review noted that the shielding plates were tightly attached to the heads with several strong bolts. Such an attachment is not prototypic and results in a stiffer head structure. In addition, it was conjectured that when such a head domes upward, the gaps between the shielding on each of the plugs close up and may lead to a potential lockup mechanism that could resist further upward deformation of the head. The heavy bolts could enhance this lockup mechanism by resisting in-plane displacements and unrealistically inhibiting head deformation.

The SDOF analysis excluded the lockup mechanism and the effect of tightly bolting the shielding to the head. Instead. it assumed that the bending stiffness of the head cross section was the sum of the stiffnesses of the head and the three layers of shielding.

Because the prototypic shielding is not tightly fastened to the head, it is possible that during slug impact, larger head displacements could occur than were measured on SM 5. The SDOF analysis, lacking experimental data on the stiffness of the prototypic head with a flexible shielding attachment, should be regarded as a means of providing an estimate of the deflection and probably a useful upper bound.

---

[2] Biggs, J. M., "Introduction to Structural Dynamics," McGraw-Hill Books, Co., New York (1964).

* This deflection was obtained after calculation errors in Reference 1 were corrected. The calculations also include analytical improvements.

B. Objectives

The objectives of the static experiments described and analyzed in this report are to determine the effect of shielding on the pressure-deflection relationship of the CRBR head, to evaluate the deflection measurement made on the dynamic test SM 5 using realistic data on head stiffness, and to provide data that allow a prediction of the head deflection under HCDA slug impact loading of a CRBR head with more prototypic shielding.

C. Approach

To meet these objectives, we implemented a program that consisted of the following four steps:

(1) Determine the static load-deflection relationship of the complete SM 5 head. (Test SM 7)

(2) Apply the SDOF analysis with this relationship to predict the SM 5 dynamic test deflection for comparison with the experimental deflection.

(3) Determine the static load-deflection relationship of a head with more prototypical shielding. (Test SM 8)

(4) Apply the SDOF analysis with this relationship to estimate the dynamic test deflection of a head with more prototypical shielding.

To this end, two static tests on 1/20-scale models of the CRBR head were performed. The three-plug heads on each model were the undamaged heads from the earlier dynamic tests SM 4 and SM 5. To one head, the undamaged shield plates with integral spacers from model SM 4 were attached with the bolts used on SM 4. This model was designated SM 7. To the other head, a new set of shield plates with separate spacer rings were attached. No permanent clamping force on the shield plates was applied to this assembly in order to simulate the prototypic thin shielding skirts that provide gravitational support to the shield plates. This model was designated SM 8. For reference, Table 1 lists the principal information about the models and tests.

Table 1

MODEL AND TEST INFORMATION

Model and Test Number*	Type of Test	Head Assembly Feature
SM 4	Dynamic	Bolted
SM 5	Dynamic	Bolted
SM 7	Static	Bolted
SM 8	Static	Stacked (prototypical)

*SM 6 is an untested model.

Each model was placed in a test apparatus that provided perimeter support identical to that provided by the vessel flange in the dynamic tests. A hydraulic pressure was applied to the underside of the shielding on each model. This pressure was gradually increased until the head failed. During the tests, head displacements were measured by electromechanical displacement gages at 17 important locations. The pressure was also measured using an electronic pressure transducer. Data from all instrumentation were recorded on magnetic tape. The analog records were digitized, and cross plots of load versus deflection were made for each displacement gage location.

The data were analyzed with two purposes in mind. First, the failure mode and failure load for each test were established. Comparisons were made to see what effects the shielding had on head response. The displacement data were also used to provide input to calculate the volume created under the head as the load was increased. Second, the load-deflection and load-volume change data were used to determine the head stiffness for each model so that relevant equivalent SDOF models for each test could be established. These SDOF models were then used to determine the dynamic response of the heads to the HCDA

slug impact loading of tests SM 4 and SM 5. The SDOF model for SM 7 was used to evaluate the dynamic response of test SM 5, and the SDOF model for SM 8 was used to predict the potential dynamic response of a more prototypic CRBR head model to the same HCDA load measured in test SM 5.

II TEST PROCEDURES

A. Head Designs

In Tests SM 7 and SM 8 we used the undamaged heads from dynamic tests SM 4 and SM 5, respectively. Figure 3 shows a schematic plan and cross section of model SM 7 in the static-test fixture. The setup for SM 8 was the same except for the shielding. The undamaged head, shielding, and shear rings from SM 4 were reassembled to the same specifications and tolerances as in Test SM 4, including the attachment bolts. For model SM 8, the undamaged head and shear rings from SM 5 were reassembled, and new shield plates and shield spacer rings were attached to the underside of the head. An outer support ring for each head was machined from A-533B steel to provide the same geometrical and strength restraints of the vessel flanges in tests SM 4 and SM 5. Precautions were taken to ensure the proper fit of the shear rings into the shear ring grooves.

B. Shield Designs

Figure 4 shows the primary differences in shield plate design between SM 7 and SM 8. On SM 7, the three A36 steel shield plates had spacers that were an integral part of each shield plate. Figure 5(a) shows the bottom layer of shield plates and spacers for SM 7. The spacing rings of the SM 8 model are typically segmented rings that are lightly bonded with epoxy to the shield plates for assembly purposes only. The spacing rings also have a much smaller cross section than those on the SM 7 model. Figure 5(b) shows the bottom layer of shield plates and rings for SM 8. Note that the size of the spacers on SM 7 would affect the bending stiffness of these plates, whereas the thin spacing rings on SM 8 would have a minimal effect on the shield plate stiffness. Also note that more penetration holes are included in SM 8 to model the CRBR shield plates more prototypically.

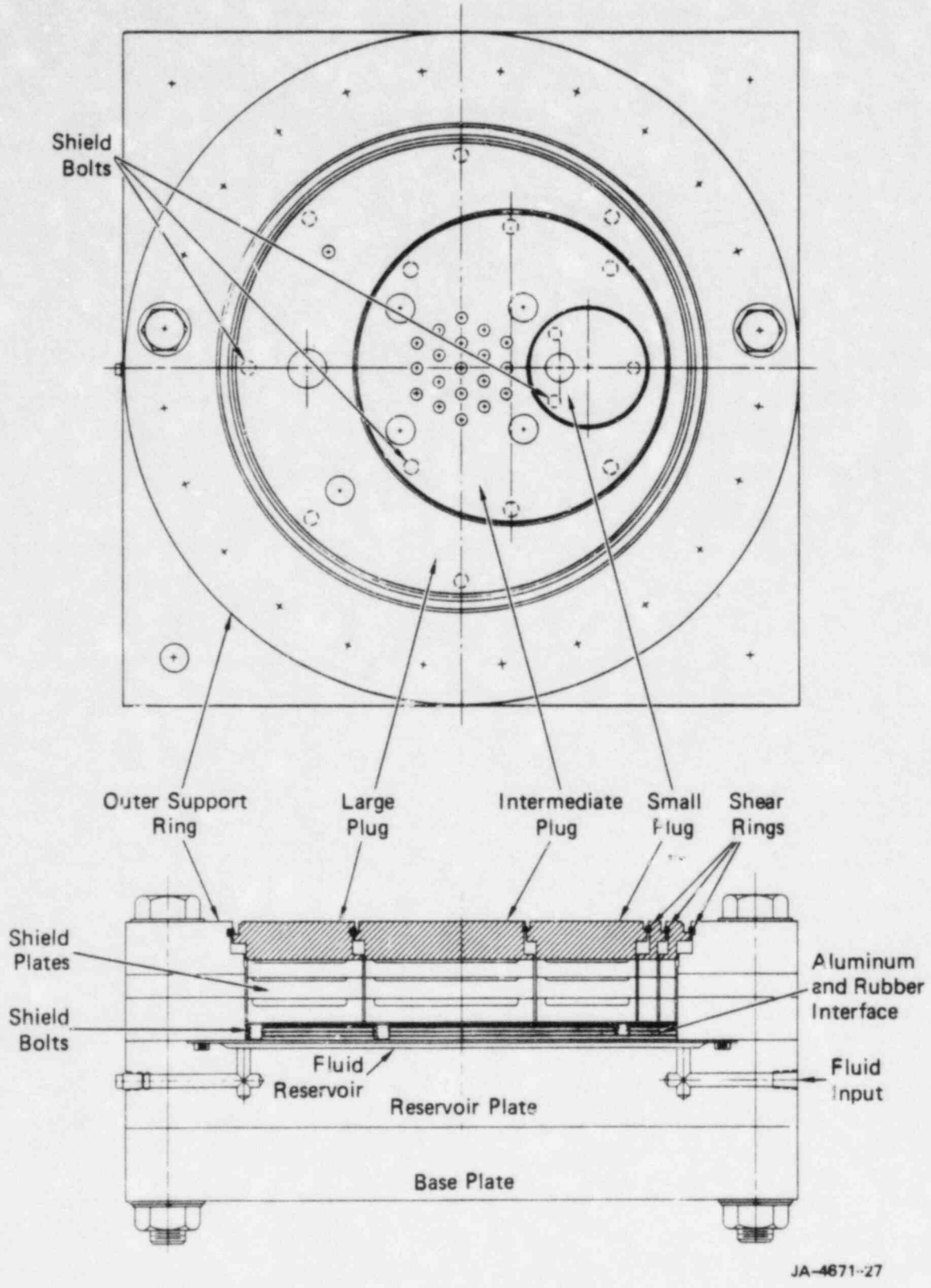

FIGURE 3 SCHEMATIC OF TEST FIXTURE FOR SM 7

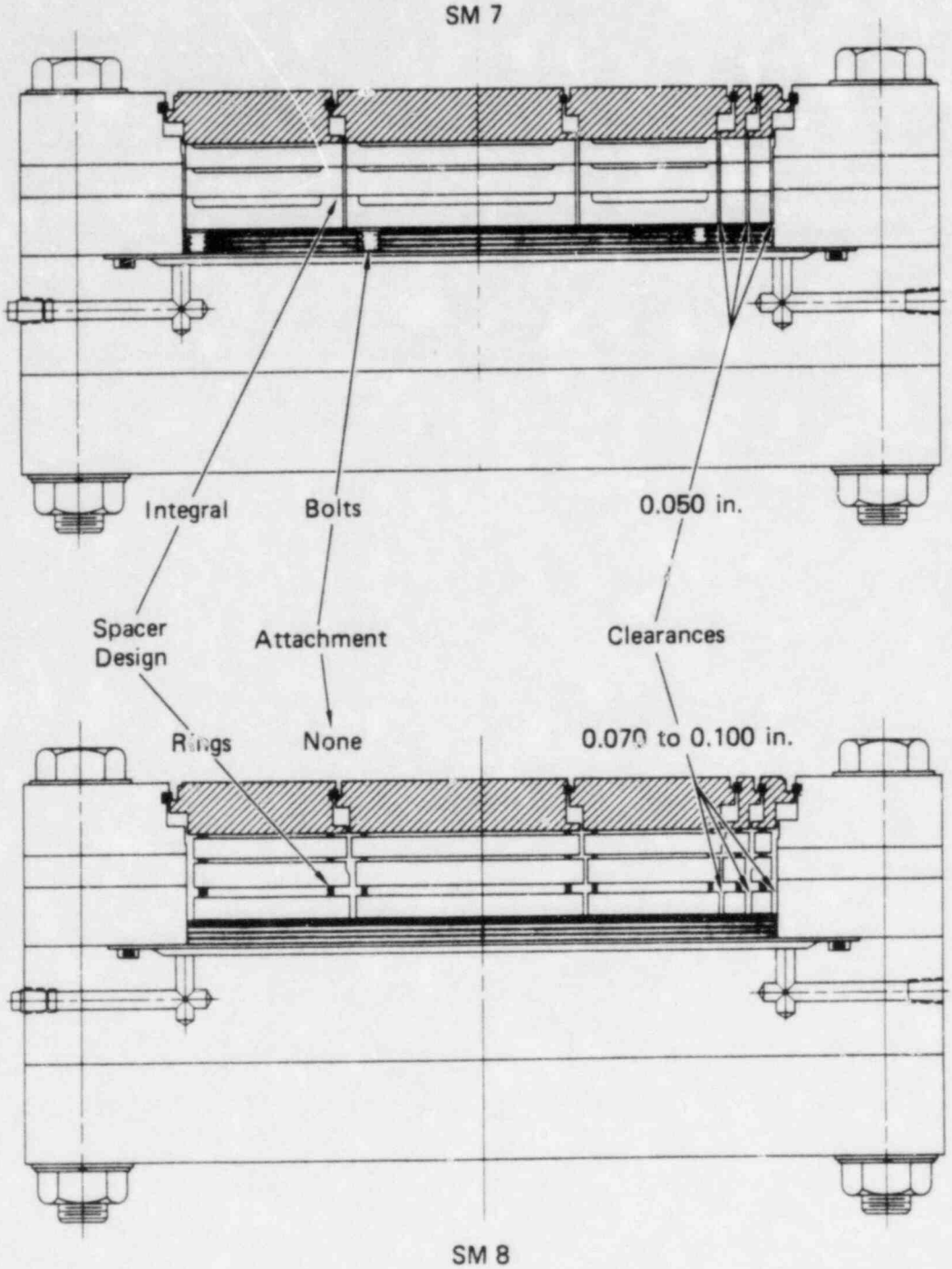

FIGURE 4 DIFFERENCES IN SM 7 AND SM 8 SHIELD PLATE DESIGNS

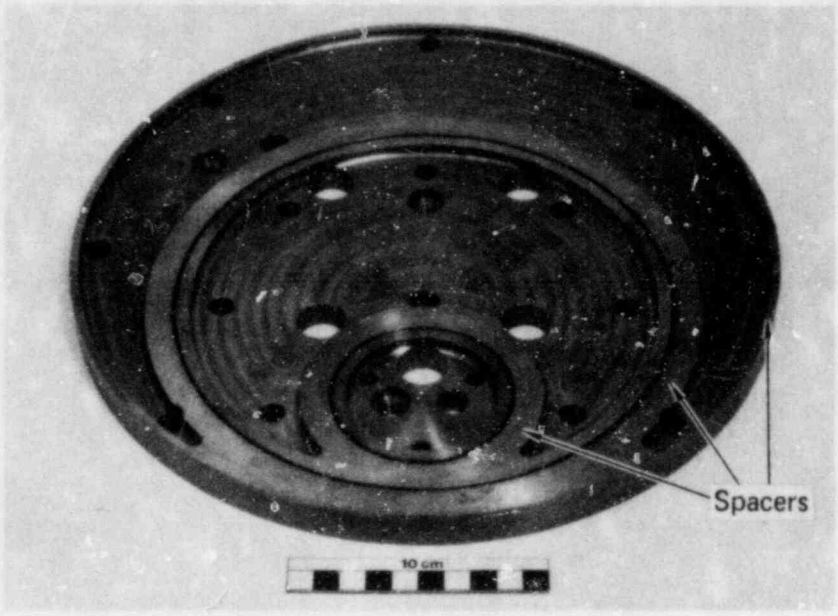

(a) Bottom layer of shield plates for SM 7

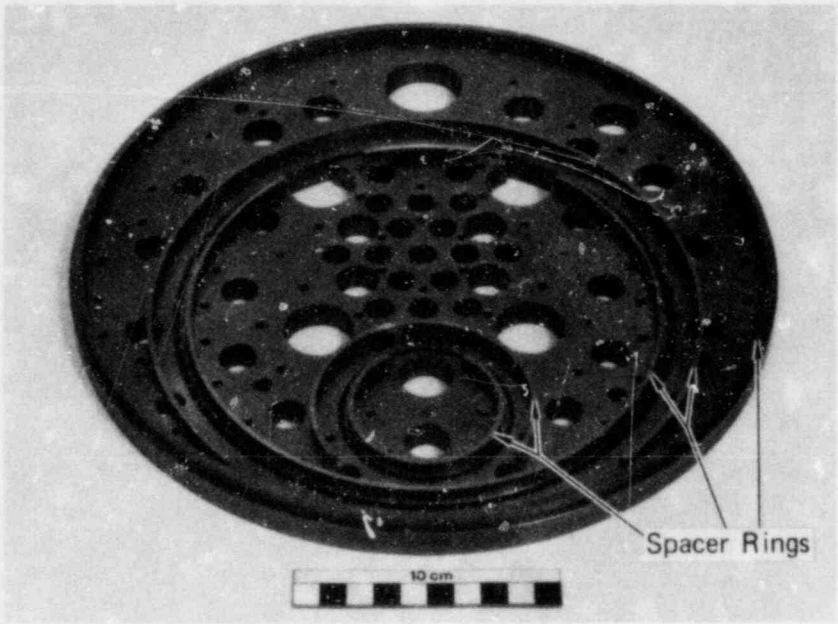

(b) Bottom layer of shield plates for SM 8

JA-4671-23

FIGURE 5 SHIELD PLATE DESIGNS FOR SM 7 AND SM 8

Another difference between shield plate designs for SM 7 and SM 8 is the gaps or clearances around the perimeter of the shield plates. On SM 7, the clearances are uniformly 0.050 inch between shield plates on the large rotating plug (LRP), intermediate rotating plug (IRP), and small rotating plug (SRP). On SM 8, the clearances are 0.100 inch between the LRP and IRP and 0.070 inch between the IRP and SRP. The differences in clearances between shield plates for the SM 7 and SM 8 models may influence head response. The larger clearances on the SM 8 model permit larger upward displacements before shield contact occurs. This contact occurs when the gaps between the bottom shield plates close up, thereby making further doming of the head more difficult. It is important to know whether closure affects head failure.

The third difference between shield plate designs is the method of attachment to the head. On SM 7, the shield plates for the LRP and IRP are securely attached to the head with seven 0.375-inch-diameter bolts on each plate torqued to near the yield strength of the bolts. The SRP shield plates are attached to the head by three 0.250-inch-diameter torqued bolts. The combined head and shield plate structure thus deforms as a single unit until the frictional forces supplied by the bolts are overcome to permit in-plane sliding between the layers of shielding. On SM 8, the shield plates are held in place initially by four small-diameter bolts. These bolts ensure proper alignment before testing. Just before the test, a small pressure (~5 psi) is applied to the underside of the head and the bolts are removed. On this model, therefore, there are initially no frictional forces to resist in-plane sliding between layers of shielding.

C. Loading Apparatus

The head structures were loaded by means of hydraulic pressure applied to the underside of the shield plates. Figure 6 shows the loading fixture and part of the hydraulic system. The loading fixture consisted of an outer support ring, shim rings to account for the thickness of the models, a reservoir plate, a base plate, and twenty-four

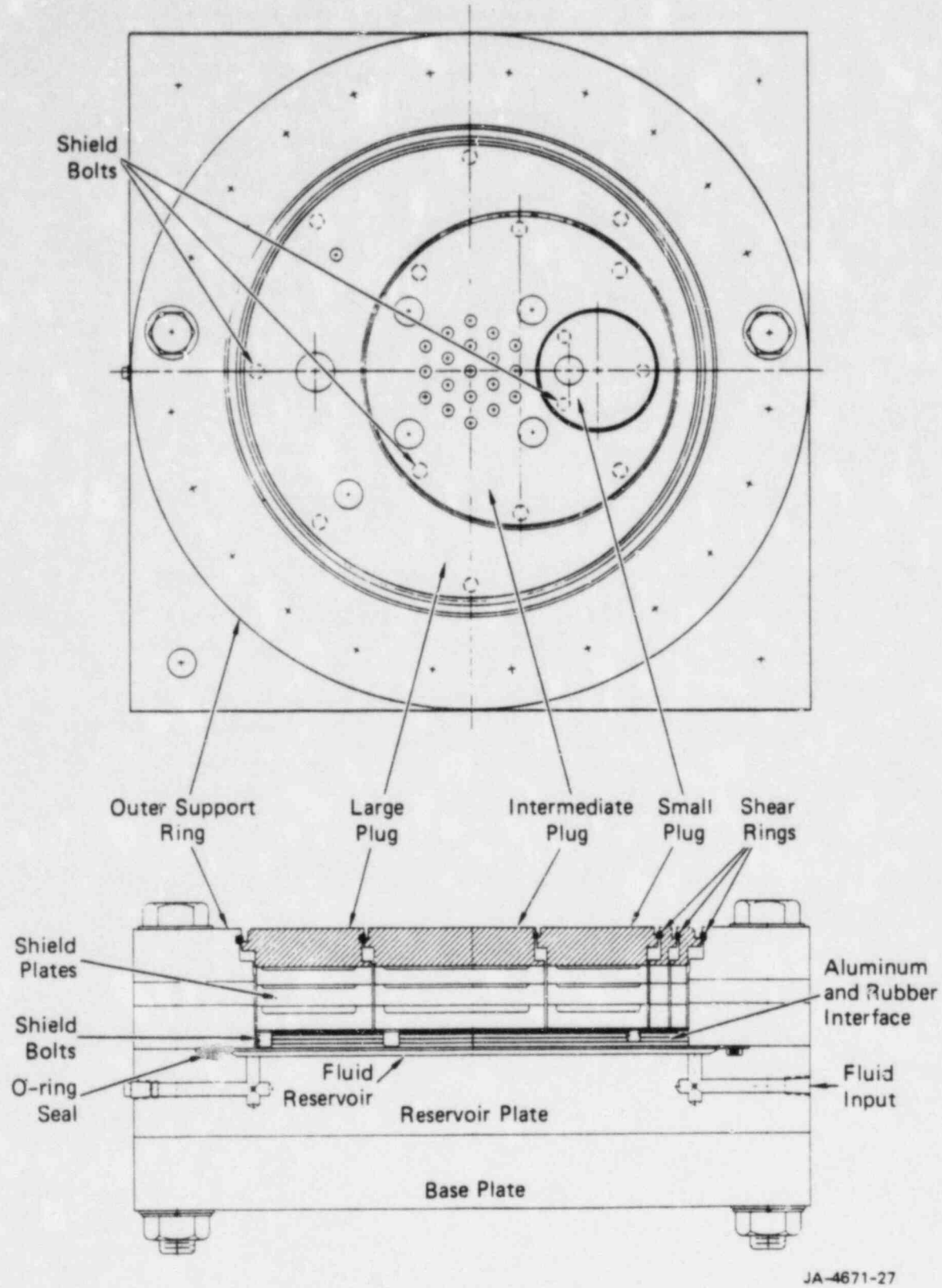

FIGURE 6 SCHEMATIC OF TEST FIXTURE FOR SM 7

1-inch-diameter bolts to hold the fixture together during loading. The reservoir plate has inlet and outlet ports for the hydraulic fluid and a dish-shaped reservoir directly under the head. This reservoir is sealed by means of a rubber diaphragm between the head and the fluid and by an O-ring around the perimeter of the reservoir. The rubber diaphragm was reinforced by an 0.032-inch-thick soft aluminum (Type 1100-0) disk. To accommodate the space between the bottom shield plate and the reservoir on model SM 7 created by the bolt head thickness, three layers of silicone rubber and two layers of soft aluminum were lightly bonded to the underside of the shielding. This laminated layer of soft material had no effect on the structural response of the head, but made direct measurement of the volume created under the head as it deformed difficult. Even though the SM 8 head had no bolt heads below the shield plates, the same layers of silicon rubber and soft aluminum were used to provide the same loading geometry as in test SM 7.

The base plate was added to strengthen the reservoir plate. In this way, deflections of the reservoir plate would not increase the apparent volume change under the head as it was loaded.

The twenty-four 1-inch-diameter bolts were designed to prevent upward displacement of the outer support ring. The high-strength bolts were torqued to a preload corresponding to a 5000-psi pressurization of the head. During a test, the preload in the bolts limited displacement of the outer support ring to less than 0.001 inch.

The loading fixture was supported on a steel table frame about four feet off the floor to provide easy assembly of the test parts.

The hydraulic system, shown in Figure 7, consisted of a hydraulic accumulator actuated by a high pressure gas, a fluid reservoir, tubing and valves, and a control panel to regulate loading. The hydraulic accumulator (Figure 8) operates by increasing the gas pressure on one side of a piston. On the other side of the piston, the hydraulic fluid (low-viscosity oil) is also pressurized, providing the load for the head. As the head deforms, the fluid leaves the accumulator to occupy the volume created under the head. As the fluid leaves the accumulator,

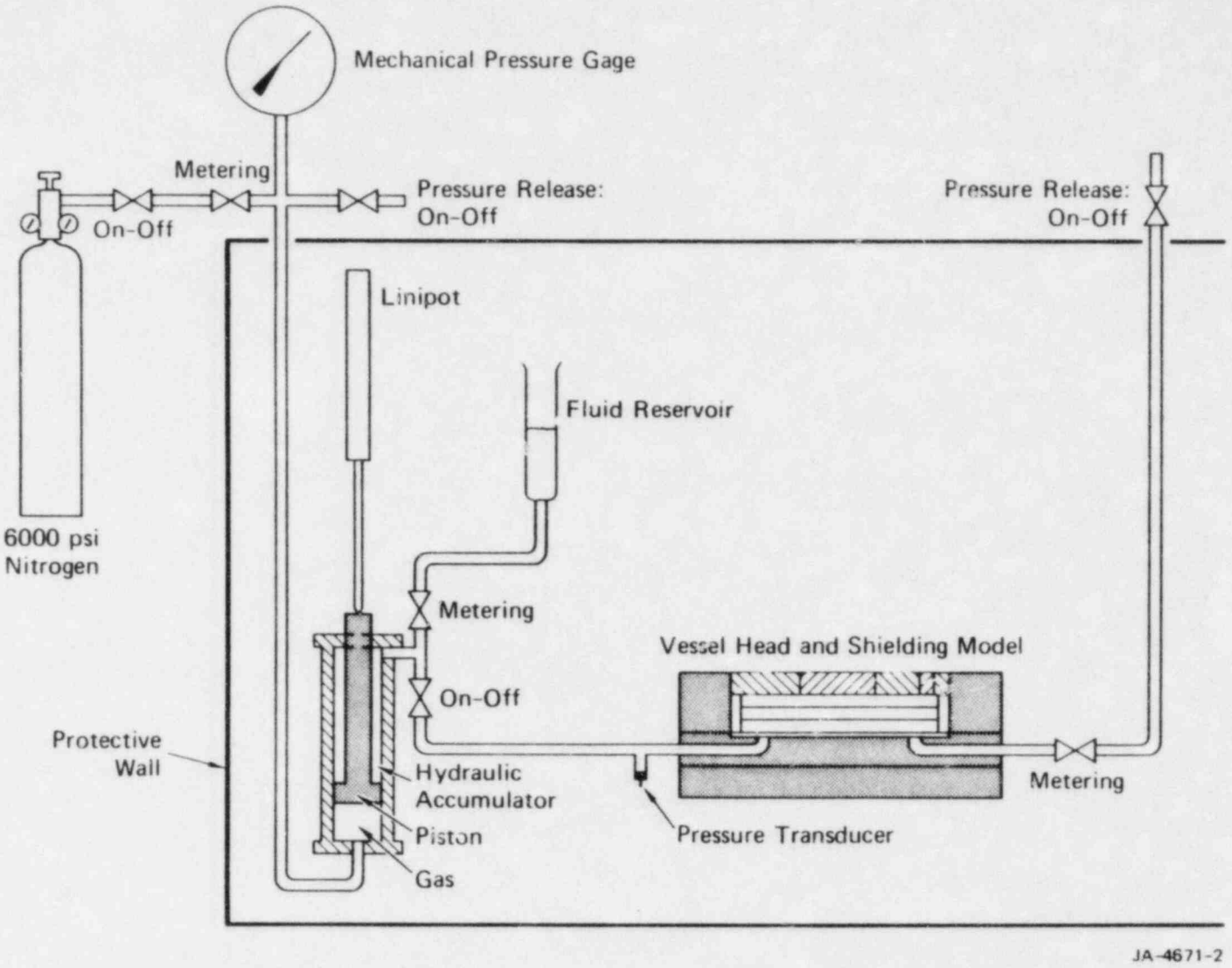

FIGURE 7 SCHEMATIC LAYOUT OF TEST AREA

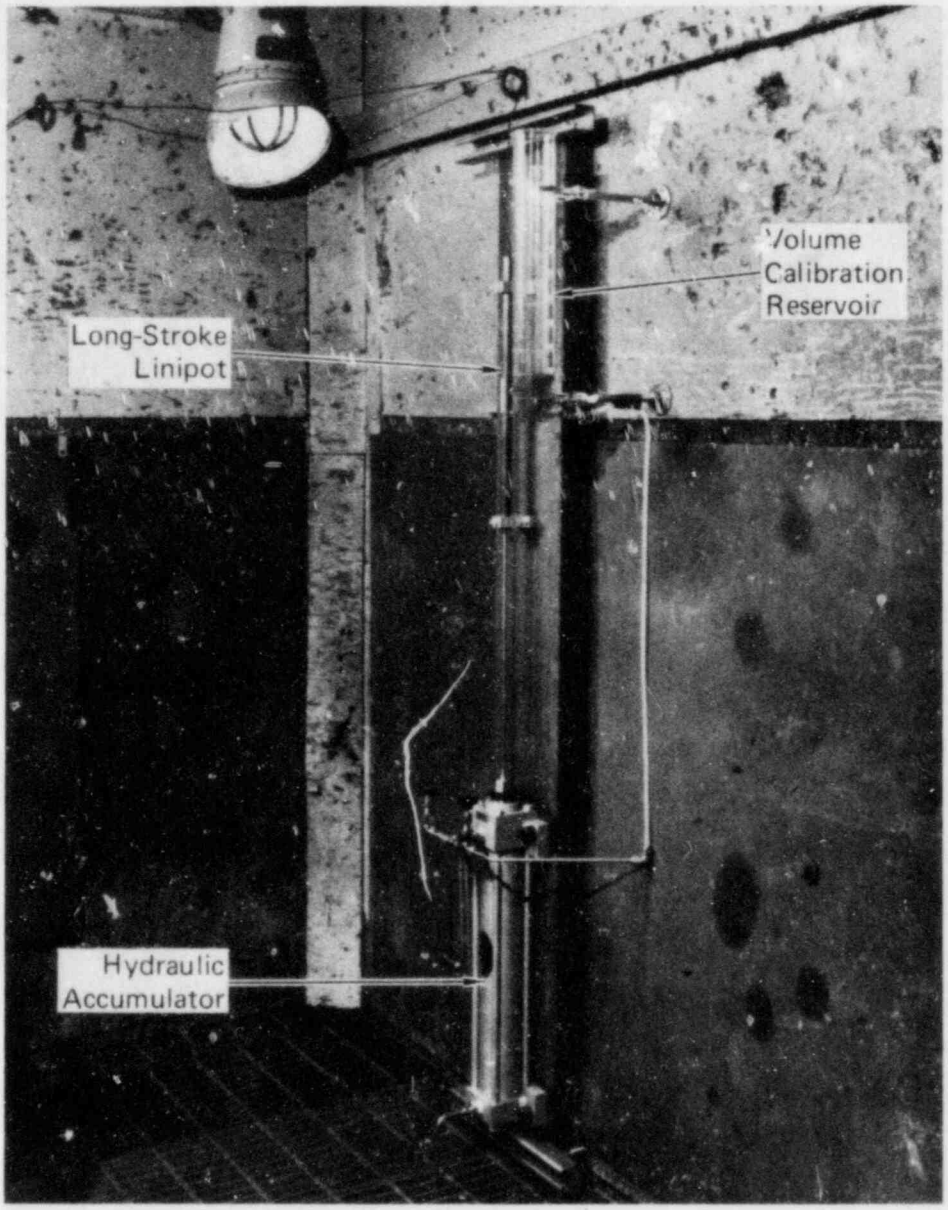

JP-4671-25

FIGURE 8 HYDRAULIC LOADING APPARATUS

the piston moves. A shaft attached to the piston is monitored by a displacement transducer (linipot) (see Figure 8). Motion of the piston is directly related to the volume of fluid forced under the head and therefore provides a measure of the volume under the head as it deforms.

A mechanical pressure gage was used to measure the gas pressure, and an electronic pressure transducer was used to measure the hydraulic pressure. A needle valve and a pressure regulator on the gas side of the hydraulic ram (Figure 7) were used to control the loading rate of the head. This control was adjusted to limit the loading rate to about 5 psi/s.

D. Instrumentation

Each model was instrumented with 17 displacement gages, one pressure transducer, and one displacement gage to measure the stroke on the hydraulic accumulator to obtain a volume change measurement. Figure 9 shows the location and numbering for each of the 17 displacement gages. The gages were numbered and placed in the same locations on SM 7 and SM 8 as were the gages on SM 1. Three types of displacement gages were used. Linear potentiometers (linipots*) were used in areas where large deflections were expected. The accuracy of these gages was ± 2 mils. Linear variable differential transformers (LVDT†) transducers were used in areas where smaller deflections and higher resolutions were needed. The LVDTs are accurate to within ± 1 mil. Table 2 lists gage number and gage type. The gages were positioned over the test fixture by means of a rigid instrument tree. The tree had holes drilled in it at the desired locations and the bodies of the gages were clamped in these holes. Spring-loaded rods were attached to the shafts of the gages, and these rods were positioned on the precise measurement locations on the models. Figure 10(a) is a photograph of the overall test setup on a

---

*Model 5184, manufactured by Bourns Instrument Division, Riverside, CA.

†Model 250-HMR and Model 100-HMR, manufactured by Schaevitz, Camden, NJ.

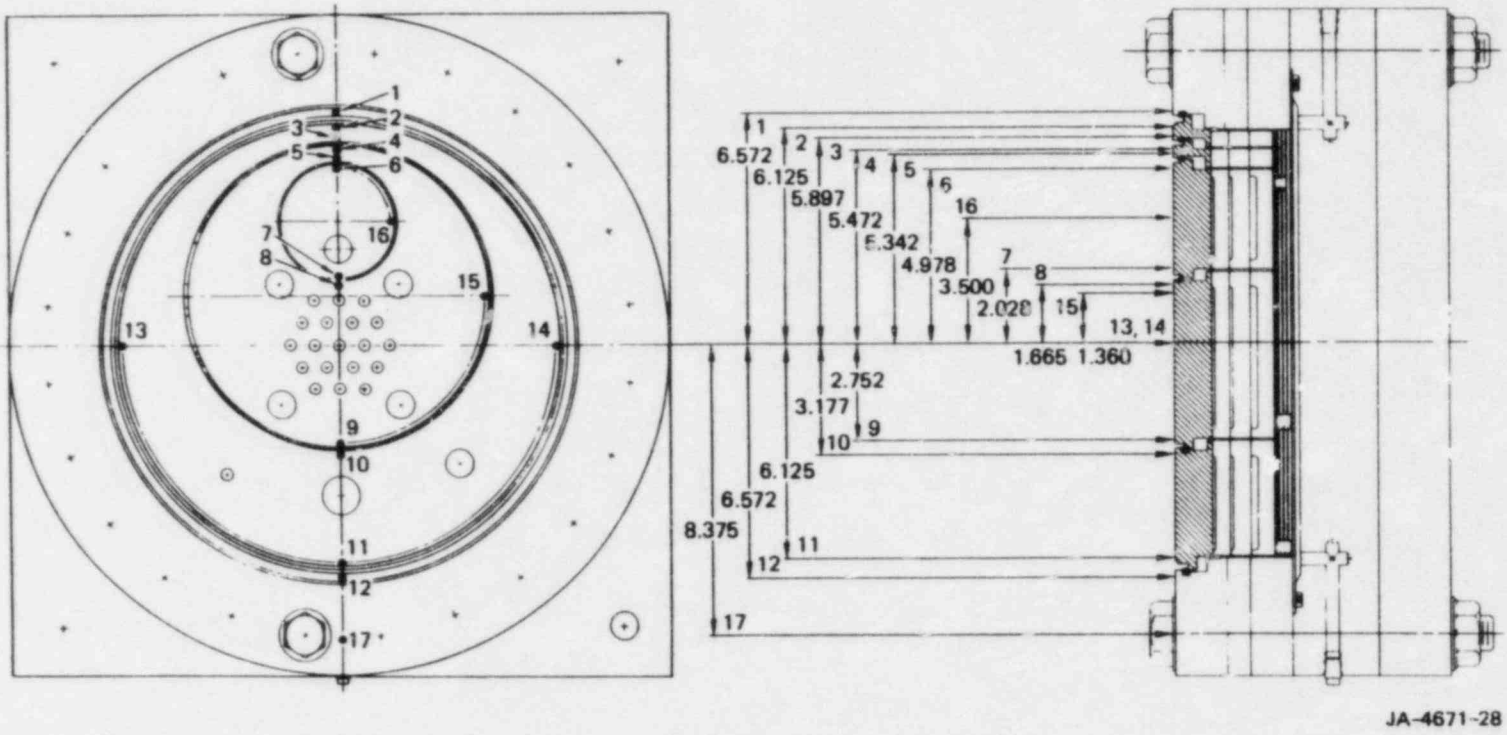

FIGURE 9 INSTRUMENTATION LAYOUT FOR TESTS SM 7 AND SM 8

Table 2

DISPLACEMENT GAGES FOR SM 7 AND SM 8

Gage Number	Gage Type	Range (mils)	Accuracy (mils)
1	LVDT	0-100	± 1
2	LVDT	0-100	± 1
3	LVDT	0-100	± 1
4	LVDT	0-250	± 1
5	LVDT	0-250	± 1
6	LVDT	0-250	± 1
7	Linipot	0-500	± 2
8	Linipot	0-500	± 2
9	Linipot	0-500	± 2
10	Linipot	0-500	± 2
11	LVDT	0-100	± 1
12	LVDT	0-100	± 1
13	LVDT	0-100	± 1
14	LVDT	0-100	± 1
15	Linipot	0-500	± 2
16	LVDT	0-250	± 1
17	LVDT	0-100	± 1

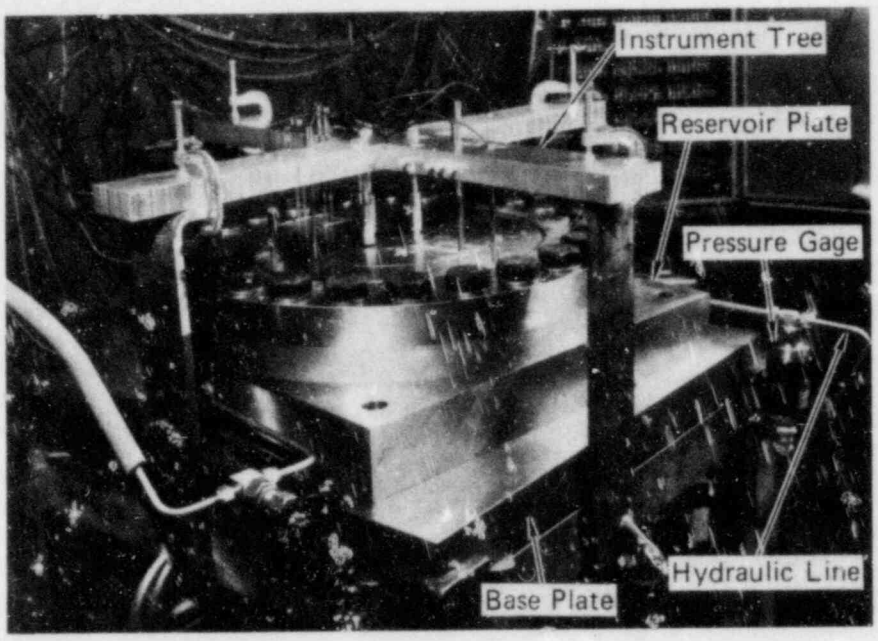

(a) Test Fixture with Instrumentation

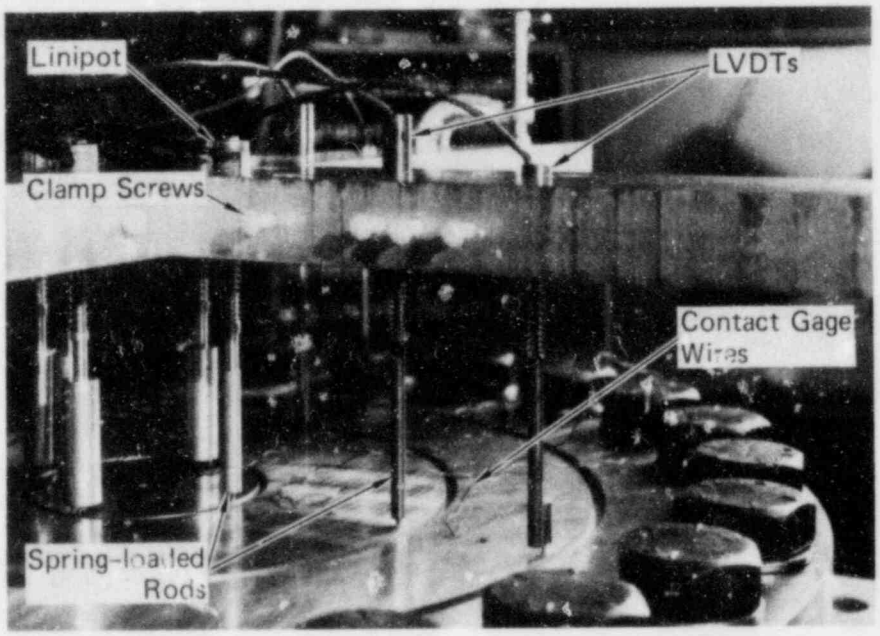

(b) Instrumentation Setup

JP-4671-24

FIGURE 10 TEST FIXTURE AND INSTRUMENTATION

preliminary experiment designed to test the loading and instrumentation techniques. Figure 10(b) is a closeup of the instrumentation tree, the gages, and the spring-loaded rods.

Figure 10(b) also shows wires leading from the head. These wires were connected to contact gages bonded to the edges of the bottom layer of shielding between the LRP and IRP and between the IRP and SRP. These gages were intended to signal if and when the bottom shield plates contacted each other.

An electronic pressure transducer* was installed in the hydraulic line leading from the accumulator to the test fixture to measure. It measured the hydraulic pressure on the underside of the head as it deformed.

A long-stroke linipot† measured the piston stroke of the accumulator. We had planned to use the data from this gage to determine the volume created under the head as it deformed. However, the experimentally determined volume from measurement of the fluid volume leaving the accumulator was inaccurate because of the compressibility of the rubber layer placed between the fluid reservoir and the lowest shield plate. Therefore, we used deformation profiles to calculate the volume under the deformed head.

Data from all gages (a total of 23 channels) were recorded on two analog tape recorders for later playback and data reduction. Selected key gages were monitored during the test for a quick evaluation of the test outcome.

E. Data Reduction

The analog records for each gage were electronically filtered at about 20 Hz to remove background noise. This low-frequency filter did

---

*Model P2G (10,000 psi), manufactured by Celesco, Canoga Park, CA.

†Model 5194, manufactured by Bourns Instrument Division, Riverside, CA.

not attenuate the signals because they were recorded over a period of 7 minutes. The filtered signals were digitized by an analog-to-digital (A/D) device that is part of a digital oscilloscope.* Digital records were stored on floppy discs for processing on a computer.

The final plots of load versus deflection were obtained by cross plotting the pressure-time history with the deflection-time history and eliminating the time in the process. Figure 11 shows an example of the technique used to obtain the final load-deflection record. This technique produced smooth and accurate records that were processed and plotted by computer hardware. Because of the difficulty encountered in trying to measure the fluid volume required to deform the head, the volume was calculated from the head deflection profiles.

*Model 2090-3, manufactured by Nicolet Instruments, Madison, WI.

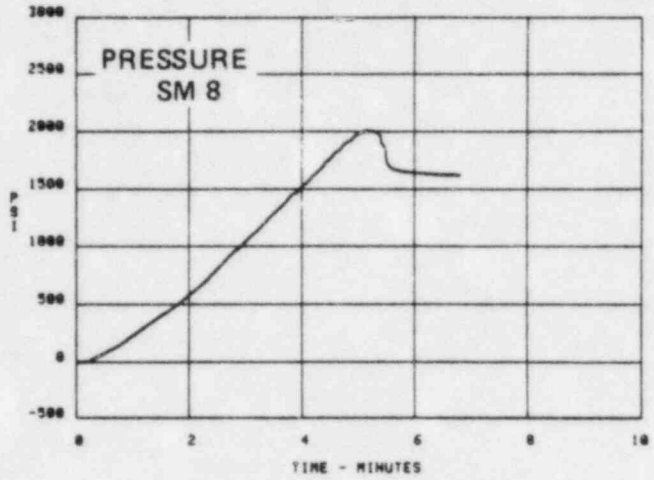

(a) Pressure-time history

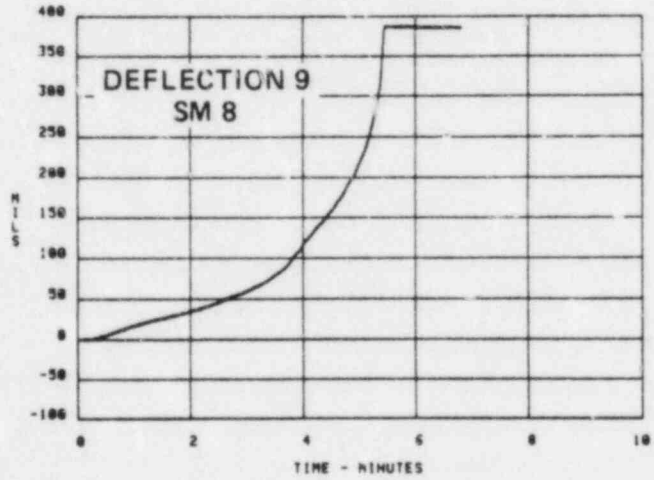

(b) Deflection-time history

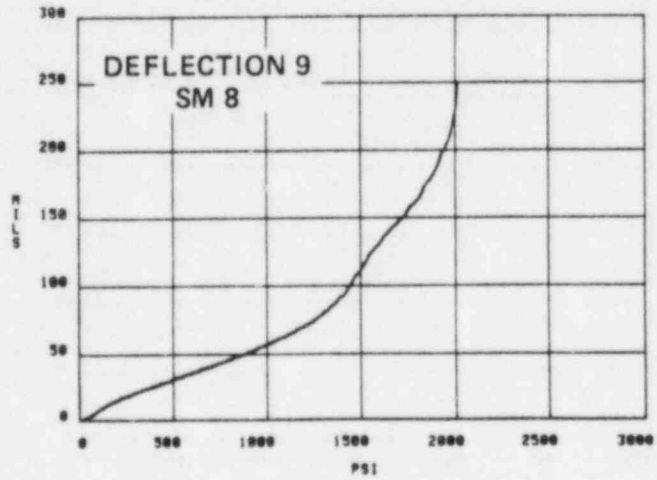

(c) Load-deflection record

JA-4671-31

FIGURE 11 DATA REDUCTION TO OBTAIN LOAD-DEFLECTION RECORDS

III TEST RESULTS

A. General Results

Models SM 7 and SM 8 were loaded to failure, which is defined here as the inability of the head to carry additional load. On SM 7, the failure load was 2587 psi and on SM 8 the failure load was 2010 psi. Differences in these failure loads reflect the effects of differences in the shielding designs and attachments. Because of the large, integrally machined spacers and strong bolt attachment of the shielding to the SM 7 head, this model was stiffer than the SM 8 model. Throughout the SM 7 test, the load required to produce a given displacement at any point on the head was larger than the load required to produce the same displacement at the comparable location on the SM 8 head.

On each test, the failure mode was the same. Failure occurs when the shear ring in the LRP begins to slip off the shear-ring-bearing surface on the IRP nearest the center of the head (displacement gages 9 and 10 location). Figure 12 shows two photographs of the final deformed shape of SM 7. The point of disengagement between the LRP and IRP is noted. Disengagement is caused by a geometrical instability rather than a material failure. Therefore, the displacement at which disengagement occurs is largely independent of the shielding design. Because of the asymmetry of the head, this disengagement is a gradual process.

The onset of disengagement was determined from the records in Figure 13 of the displacement difference across the point where disengagement begins (at the gage 9 and gage 10 locations). When the displacements begins to increase rapidly, it is assumed that disengagement has begun. For SM 7 disengagement begins at a load of 2200 psi, which corresponds to a deflection of 125 mils, and for SM 8 disengagement begins at a load of 1600 psi, which corresponds to a deflection of 130 mils. Disengagement continues until at a displacement of about 0.250 inch on each model at the gage 9 location, the head can no longer

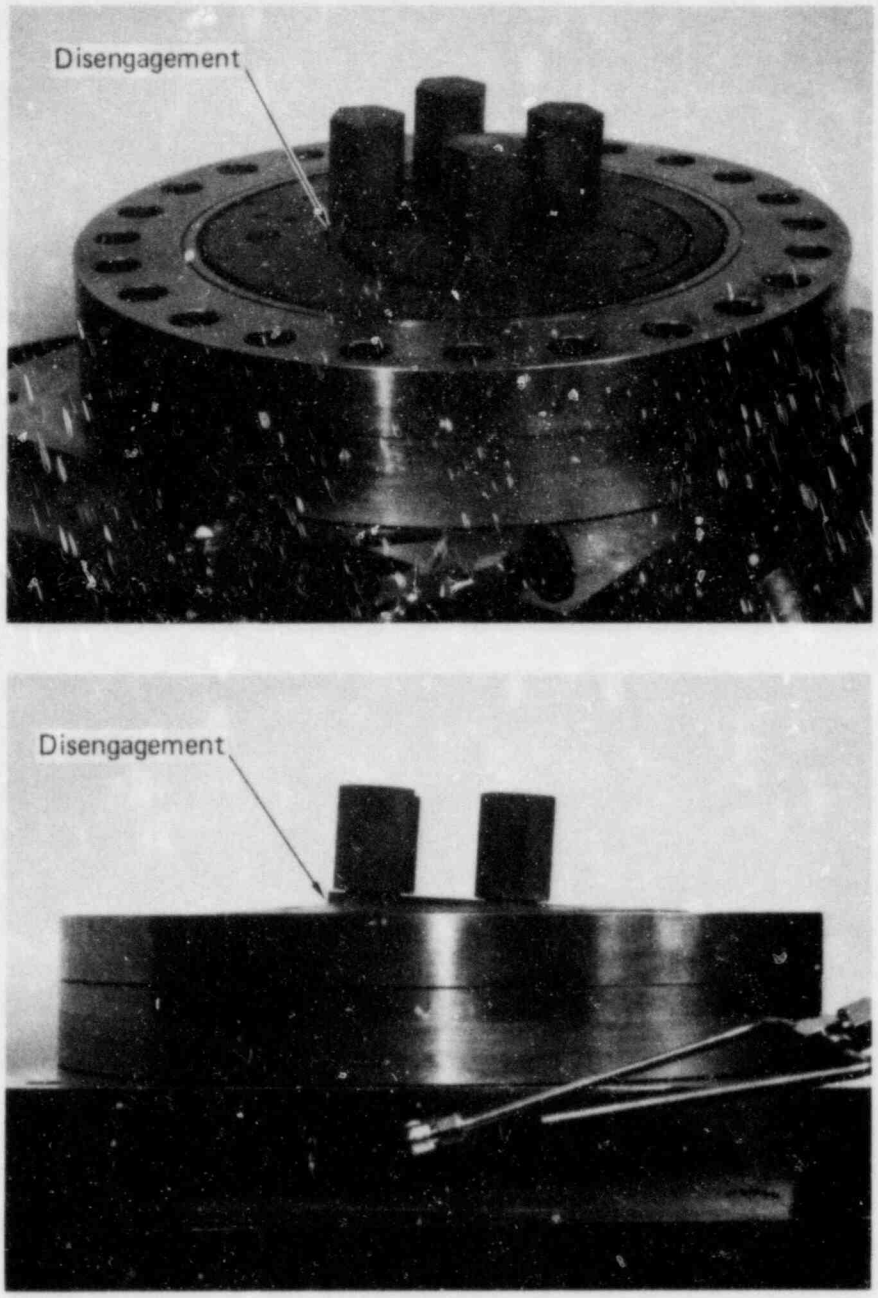

JP-4671-30

FIGURE 12 POSTTEST DAMAGE TO SM 7

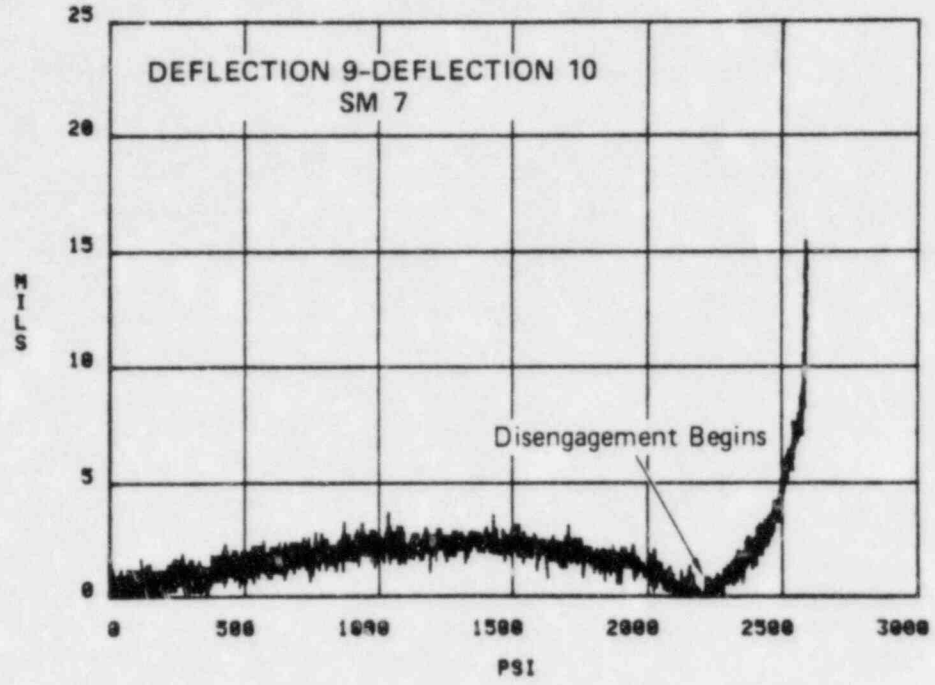

(a) Relative displacement between gage 9 and gage 10 locations for SM 7

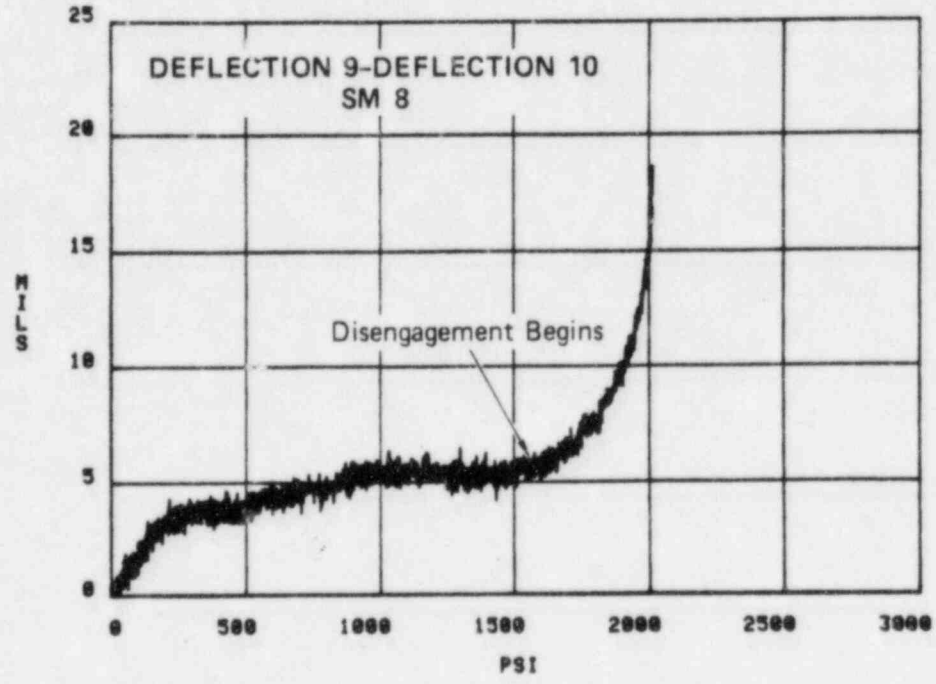

(b) Relative displacement between gage 9 and gage 10 locations for SM 8

JA-4671-32

FIGURE 13 RELATIVE DISPLACEMENTS ACROSS POINT OF DISENGAGEMENT FOR TESTS SM 7 AND SM 8

sustain pressure. Therefore, the final deformed shapes for both the SM 7 and SM 8 models are similar. The only plastic deformations on the head that are significant occur in the LRP and its shielding and on the LRP and IRP at the thin section where the plugs nest together (near displacement gages 2, 3, 4, and 5). Figure 14 is a photograph of one of the LRP shield plates from SM 7. The peak plastic displacement of the LRP is 220 mils at the edge of the cutout for the IRP.

B. Quantitative Results

Load-deflection records for all gage locations on the head are presented in Appendix A for tests SM 7 and SM 8.* Load-deflection records at the location of maximum deflection (near the LRP-IRP junction, gage 9) are reproduced in Figure 15. The SM 7 record is linear up to approximately 1500 psi, which is typical of most of the other SM 7 load-deflection records. At a pressure of about 1500 psi (50 mils displacement at the gage 9 location), the load deflection record becomes nonlinear as the result of plastic deformation of the head.

Disengagement begins at a displacement of 125 mils (2200 psi) and continues until the head fails at a peak pressure of 2587 psi. The SM 8 load-deflection records are linear between about 200 and 1100 psi (65 mils displacement at the gage 9 location) after which the head deforms plastically. Disengagement begins at a displacement of 130 mils and continues until gross disengagement of the LRP-IRP shear ring prevents further loading at a displacement of about 250 mils (2010 psi). The failure load on SM 8 is 22% lower than the SM 7 failure load.

The local stiffness of the head at each gage location is determined from the slope of the linear portion of the load-deflection records.

---

*Deflections at the gage 17 location on the outer support ring were less than one mil, therefore, the gage 17 record is not included in the appendix.

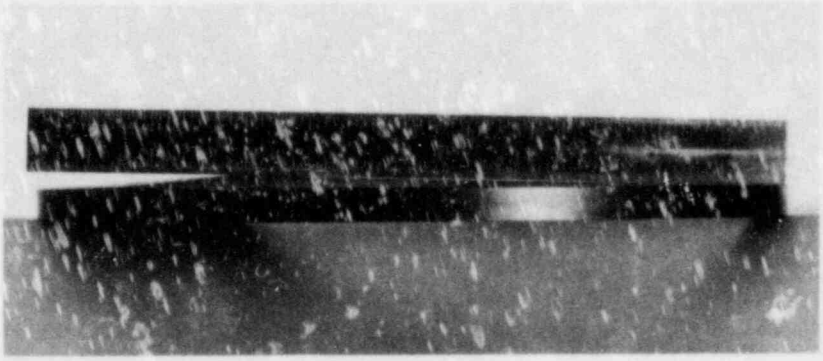

JA-4671-29

FIGURE 14 PLASTIC DEFORMATION ON SM 7 SHIELD PLATES

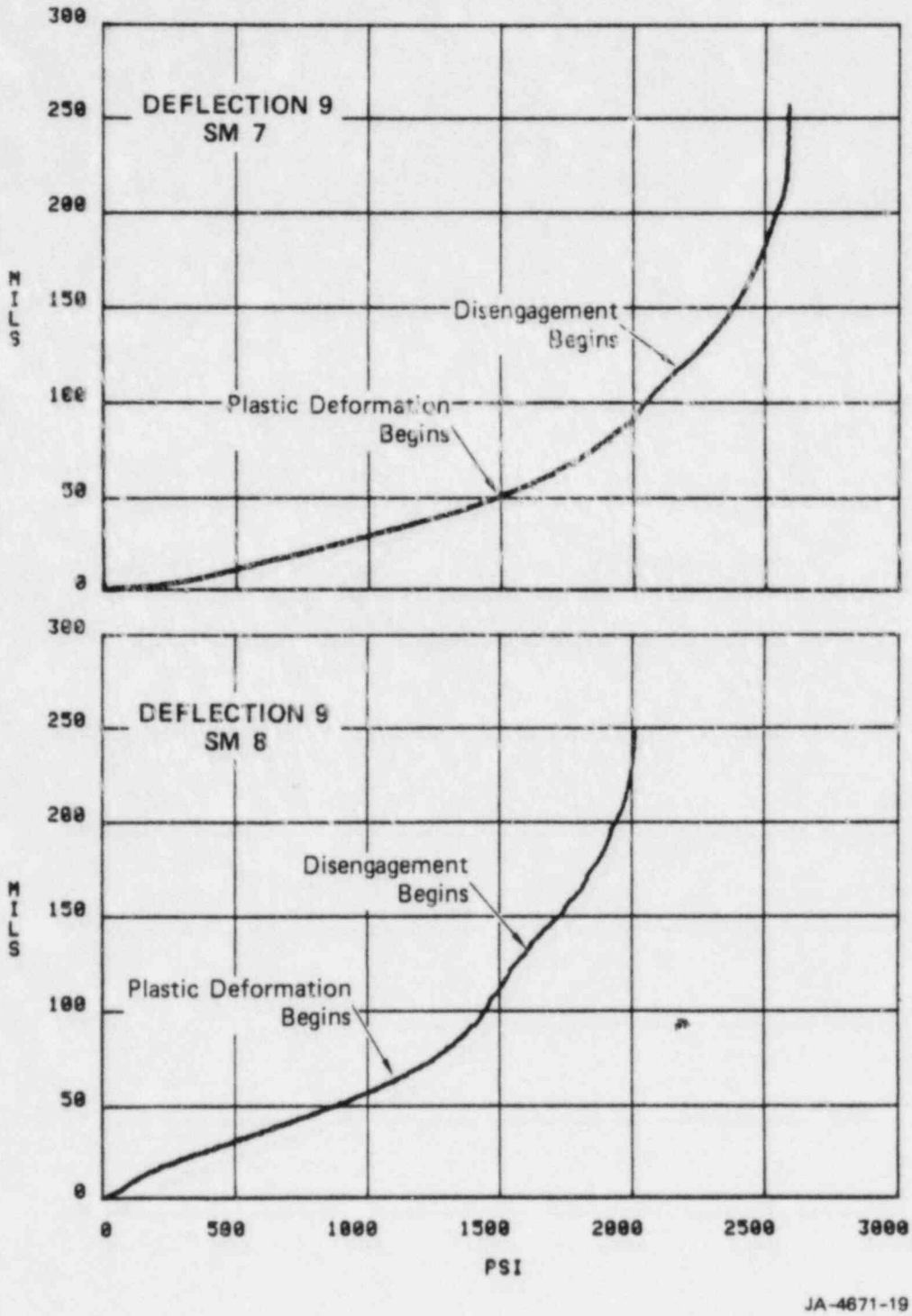

FIGURE 15 MAXIMUM DEFLECTION VERSUS PRESSURE FOR SM 7 AND SM 8

The local stiffness of SM 7 at gage 9 is 2.7×10^4 psi/in. The local stiffness of SM 8 at this same location is 2.0×10^4 psi/in., a decrease in local stiffness of 26%. The differences in local stiffnesses is attributed to the difference in shielding design and attachment between the two models.

At low pressures, the SM 8 load-deflection records indicate an initial jump in deflection. This jump is attributed to small realignment of the LRP, so that the outer support shear rings properly engage the shear-ring-bearing surface. This realignment can result in a vertical displacement of about 6 mils. An effort was made to carefully align the plugs before each test by slightly pressurizing the head before the experiment. In SM 7, the initial pressurization was effective because there were no initial jumps in deflections.

Composite plots of deformed profiles of the SM 7 and SM 8 heads along the axis of symmetry at various pressures are shown in Figures 16 and 17, respectively. The profiles were drawn by assuming the deflections varied linearly between gage locations on each plug. The difference in mode shape between SM 7 and SM 8 is the direct result of the difference in shielding attachment and shield gap sizes.

A concern in evaluating the response of the head is whether lockup occurs, and, if it does, what effect it has on the load-deflection characteristics of the head. Lockup may occur when rotation of the plugs during head deflection closes the small clearance gaps between the bottom shield plates. When the gaps are closed, further upward deflection of the head could be impeded by the in-plane forces acting at the points where the shielding comes together. If, however, the shield plates can slide when contact is made, the in-plane forces cannot build up. Because of the asymmetry of the head, contact does not occur at the same time for each plug; therefore, the shield plates slide without appreciably stiffening the head.

The contact gages on both SM 7 and SM 8 indicate that the gaps between shield plates remained open until failure. However, plug rotations calculated from the deformed shape profiles of each model

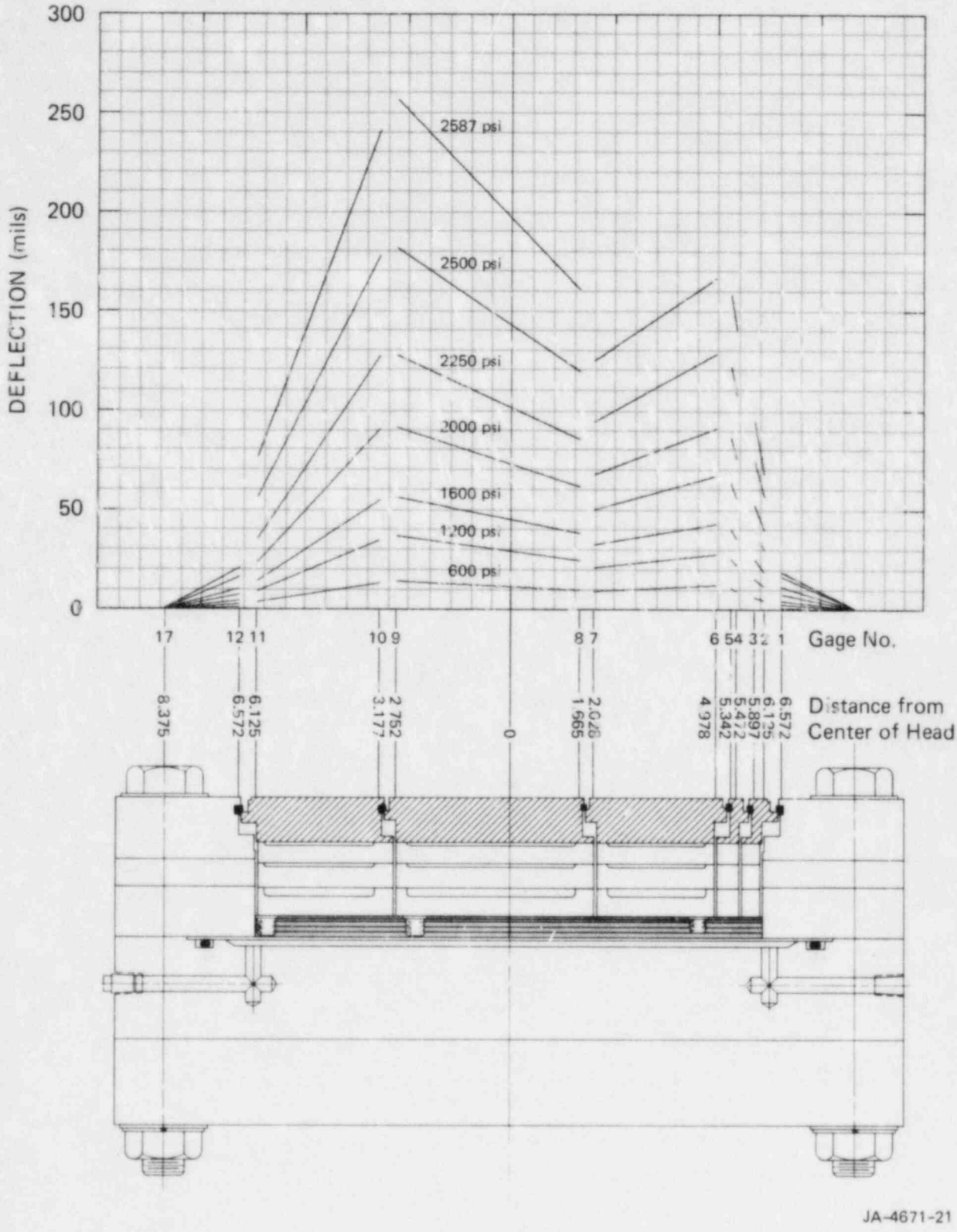

FIGURE 16 PROFILES OF HEAD AT SEVEN PRESSURES FOR SM 7

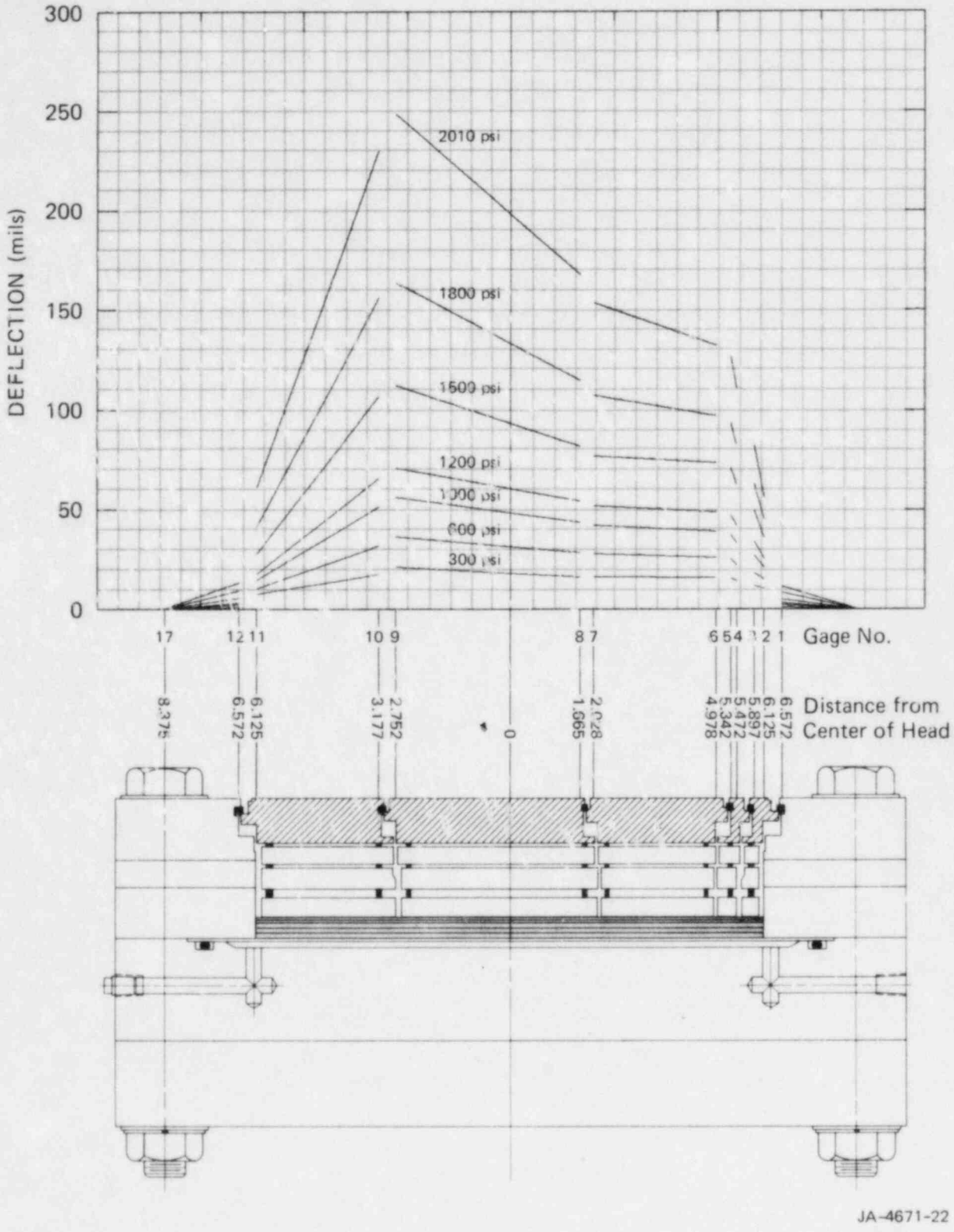

FIGURE 17 PROFILES OF HEAD AT SEVEN PRESSURES FOR SM 8

(Figures 16 and 17) indicate that the LRP-IRP shield plates for SM 7 should have touched when disengagement started at a load of 900 psi (a displacement of about 30 mils at the gage 9 location). Similarly, for SM 8, rotation calculations indicate that the shielding should have touched at the same location when the load was 900 psi (~50 mils displacement at the gage 9 location*). The gages did not register contact until head failure possibly because contact occurred slightly off axis. Because the load-deflection relations (Figure 15) show no stiffening of the heads at these displacements, we conclude that the shield plates slid to new positions as discussed earlier.

The SM 7 head profiles in Figure 16 indicate that bottom-shield contact occurred between the LRP and IRP (Gages 9 and 10) and between the SRP and IRP (gages 5 and 6). The contact forced the IRP and SRP together and caused the SRP to slide a little below the IRP (gages 7 and 8). Figure 17 shows that the SRP was not subjected to this type of displacement because of the larger gaps between the shield plates.

The volume under the deformed head was calculated using the deformation profiles at several pressures. In the calculation the three shear ring circles were assumed to remain circular. Plots of SM 7 and SM 8 pressure-volume curves are shown in Figure 18. The slope of the linear portion of the pressure-volume curve is a measure of the stiffness of the head, whereas the area under the curve is an indication of the work done in deforming the head. The slope of the SM 7 curve is 372 psi/in.^{3}, whereas the slope of the SM 8 curve is 251 psi/in.^{3}, a 33% decrease in stiffness.

In static test SM 1 of the previous experimental program,[1] the slope of the pressure-volume curve for the head without shielding was 130 psi/in.^{3}. Including the effect of the three shield layers by

---

*The larger displacement for shield gap closure is the result of a larger clearance gap between the IRP and LRP on the SM 8 model.

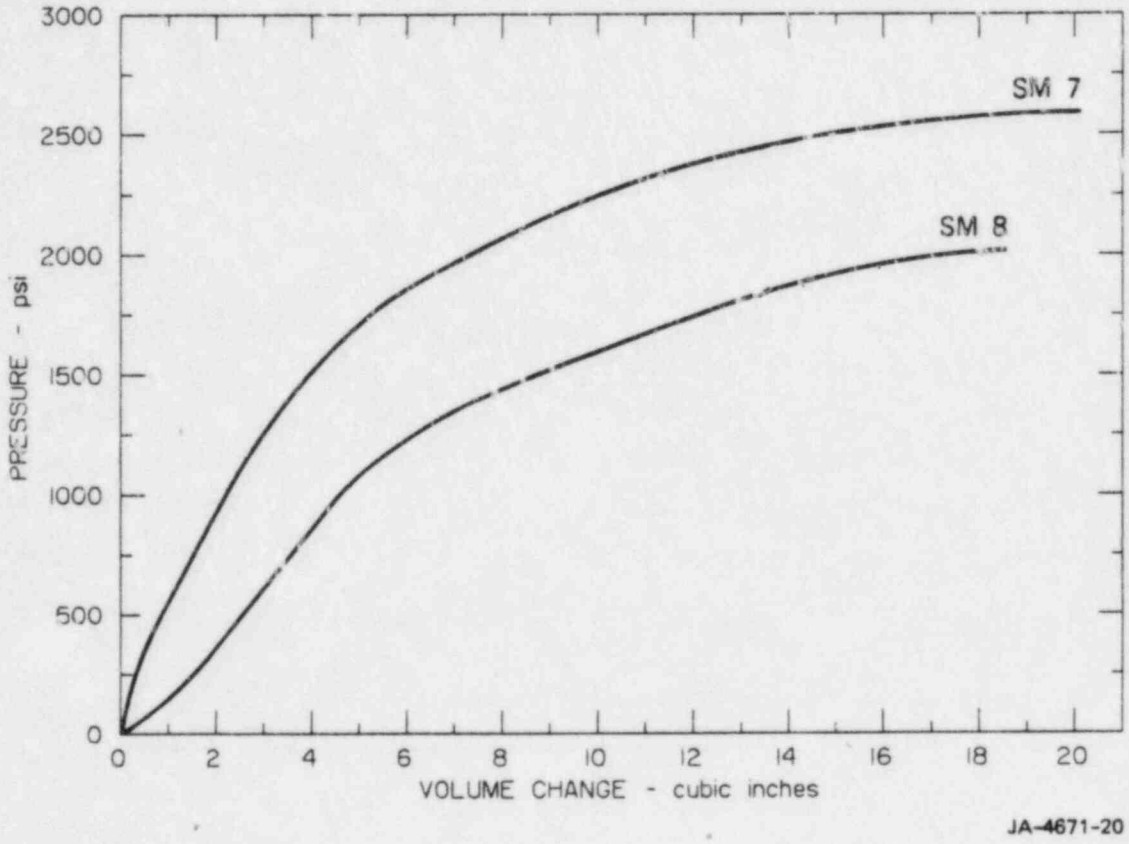

FIGURE 18 PRESSURE-VOLUME CHANGE RELATIONS FOR SM 7 AND SM 8

assuming that one shield layer slides relative to the next shield layer during bending gave a composite head stiffness of 197 psi/in.^{3} However, if the head and shield plates bend as an integral composite plate so that relative sliding of the head and shield plates does not occur, the bending stiffness would increase by a factor of 15 to about 3000 psi/in.^{3}. Both the SM 7 and SM 8 stiffness calculations exceed the lower bound of 197 psi/in.^{3}, but are close enough to this value to indicate that sliding occurs between the head and shields, with some frictional restraint.

At low pressures (between 0 and 300 psi), the initial slopes of the SM 7 and SM 8 pressure-volume curves are different. The SM 7 initial slope is approximately 1000 psi/in.^{3}, which gradually decreases with increasing pressure. The SM 8 initial slope is approximately 150 psi/in.^{3}, gradually increasing with pressure. The different initial slopes reflect the differences in shielding attachment and a small lack of alignment in SM 8. The SM 7 shield plates are attached to the head by several strong, heavily torqued bolts that preload the composite head. Because the SM 7 head and shield plates are tightly bolted, the composite head initially bends as if it were a solid plate, with limited relative sliding between the shield layers or head. As the pressure is increased, in-plane forces from bending overcome the frictional forces from the torqued bolts causing some relative sliding to occur. This relative sliding between the shields and head reduces the stiffness of the composite head, resulting in the decreasing slope of the SM 7 pressure-volume curve at low pressures. The SM 8 head and shield plates are separated from each other by spacer rings that are lightly epoxied to the shield plates. After the pressure has aligned the LRP (at a deflection of 6 mils, which corresponds to 0.75 in.^{3}), the plates slide relative to one another resulting in a stiffness near that calculated for bending of a frictionless laminar plate. As the pressure increases, frictional forces between the shield plates and the spacer rings increase to inhibit in plane sliding between shield plate layers. As this occurs, the stiffness of the head increases as shown in Figure 18.

C. SDOF Analysis for Dynamic Response of the CRBR Head

One of the program objectives is to determine the effect of shielding on dynamic head deflections. In this section, we discuss the principal points of the analyses; details of the predictive analyses are given in Appendix B.

In the initial analyses, we adopted the simplest approach. The asymmetric three-piece head was first replaced by a symmetric three-piece head having the same linear pressure-volume relationship. For SM 7 and SM 8 the slopes of the linear portions of the pressure volume curves are 372 psi/in.^{3} and 251 psi/in.^{3}, respectively. Next, the symmetric model was idealized into an equivalent single-degree-of-freedom (SDOF) system. The deflection of the head caused by slug impact loading from a 661 MW-s HCDA was estimated by calculating the dynamic response of the SDOF system. The impact load (Figure 19), which was measured on the earlier dynamic tests SM 4 and SM 5, is characterized by an initial spiked impulse of 0.38 psi-s followed by a triangular load history. The triangular load history has a peak pressure of 1200 psi that decays to zero in 1.2 ms.

For the SM 7 model, the equivalent SDOF analysis for a symmetric model of the head gave a peak elastic deflection of 87 mils that occurred 0.58 ms after slug impact. The peak deflection measured in dynamic test SM 5, which used the same method of shielding attachment as static test SM 7, was 60 mils; this deflection occurred 0.68 ms after impact.

The symmetric three-piece model was improved by adopting an asymmetric three-piece model with the same pressure-volume relation as the SM 7 test. An equivalent SDOF analysis for this model of the SM 7 head gave a peak elastic deflection of 91 mils at 0.55 ms.

In these examples, the mass of the head was assumed to be uniformly distributed over the surface of the head. However, each plug of the actual head has a different mass-per-unit-area. When this nonuniform mass distribution was accounted for in the asymmetric model, the peak dynamic deflection decreased from 91 mils to 89 mils.

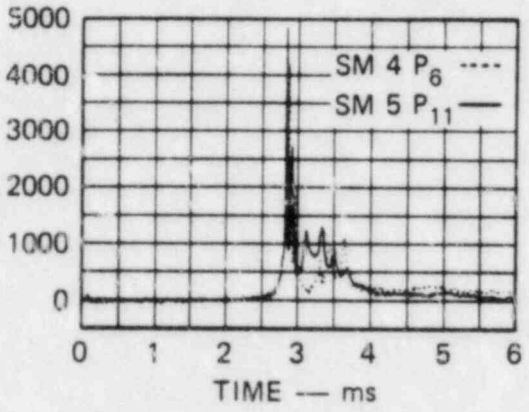

SLUG IMPACT LOAD

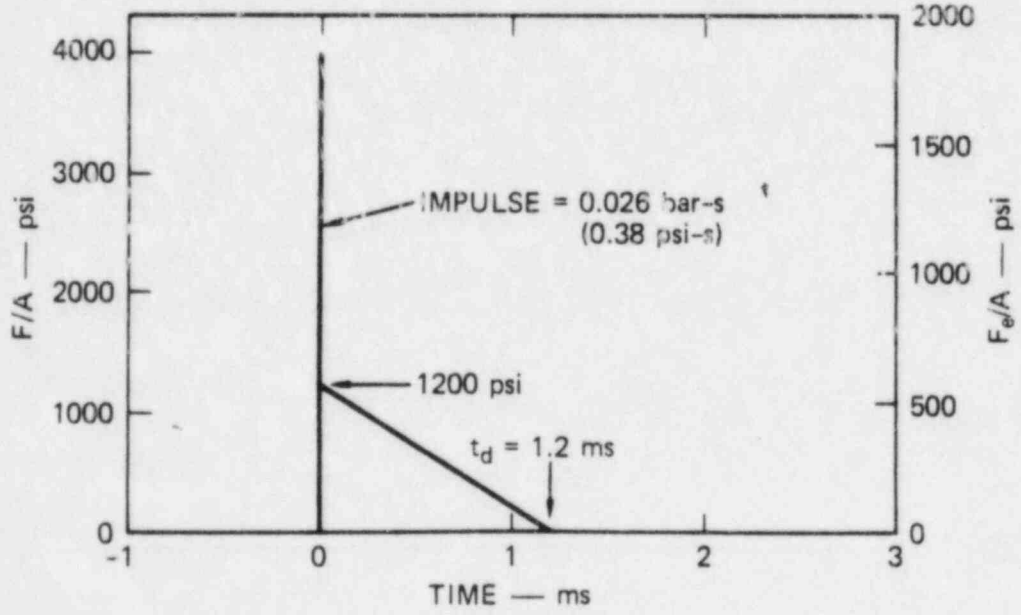

APPROXIMATION TO SLUG IMPACT LOAD

MA-3929-386

FIGURE 19 EQUIVALENT SLUG IMPACT LOAD

At these deflections (~90 mils), the load deflection curve (Figure 15) indicates that the SM 7 head has begun to deform plastically but has not reached the minimum deflection to begin disengaging (~125 mils). To account for the nonlinearity in the load-deflection curve, bilinear and trilinear approximations to the load-deflection curve were used in the SDOF analysis. The bilinear approximation was applied to include low pressure nonlinearities and to determine the influence of nonlinearities in the curve at small deflections (5 to 10 mils), the trilinear approximation was applied to determine the effects of nonlinearity when the head deforms plastically and begins to disengage. For SM 7, the predicted peak dynamic deflection became 89 mils (at 0.57 ms) for the bilinear approximation, but increased to 179 mils for the trilinear approximation. Deflections for the various SDOF models of SM 7 are shown in Table 3.

Table 3

PREDICTED PEAK DYNAMIC DEFLECTIONS
OF THE CRBR HEAD USING SDOF ANALYSIS

Geometry	Mass	P/V	Deflection (mils) SM 7	SM 8
Sym.	Uniform	Linear	82	109
Asym.	Uniform	Linear	91	111
Asym.	Nonuniform	Linear	89	109
Asym.	Nonuniform	Bilinear	89	110
Asym.	Nonuniform	Trilinear	179	202

Similar analyses were applied to the SM 8 head to predict peak deflections following a 661 MW-s HCDA slug impact. The results are also summarized in Table 3.

Because the SDOF method generally overpredicts deflections, an estimate of the overprediction was obtained by analyzing a three-piece symmetric circular plate subjected to the triangular pressure loading plotted in Figure 19 by means of the finite-element code WHAM. comparing the final deflection with the SDOF deflection gave an estimate of 16% for the overprediction. Applying this reduction to the deflection results in Table 3, when the stiffness is bilinear, gives 75 and 92 mils for SM 7 and SM 8, respectively. Similar reductions should be expected if the stiffness is represented in a trilinear form.

The SDOF analyses predict deflections for each head between the values corresponding to the bilinear and trilinear stiffness models in Table 3. The range for SM 7 is well above the deflection obtained in test SM 5, which is a clear indication that a substantial mechanism has not been included in the SDOF analysis.

D. Comparison of Test SM 5 with SDOF Predictions

In the static tests SM 7 and SM 8, plastic flow occurs when the deflection is about 60 mils, and disengagement of the LRP and IRP initiates when the deflection is about 130 mils. The SDOF analysis of SM 7 indicates that in the dynamic test SM 5 some plastic flow would occur and possibly even slight disengagement (see last two columns of Table B.3), even allowing for a crude 16% overprediction of the deflection. However, in the dynamic test SM 5, no measurable plastic strains were produced, and the maximum deflection was only 60 mils. Therefore, an important restraining mechanism was acting on the head. This restraining mechanism was caused by the upper internal structure (UIS), which was locked into the head and the upper core barrel former ring (Figure 20). After the simulated HCDA event, the UIS was still locked into the head and core ring, and the main UIS deformation was caused by axial buckling. Thus, throughout the upward motion of the head a substantial restoring moment was applied to the IRP, thereby, restricting upward deflections. Allowing for the observed UIS shortening of 170 mils, an upward IRP translation of 225 mils is required before the UIS can become

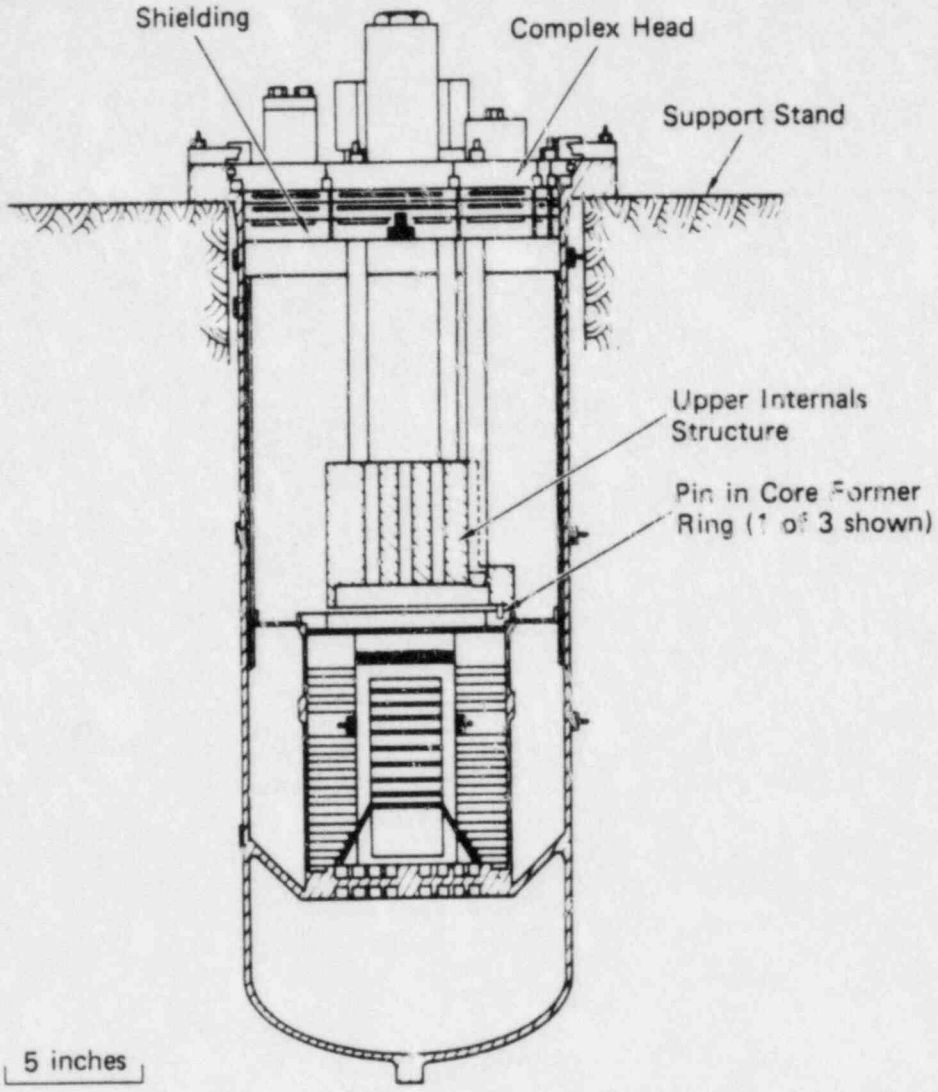

FIGURE 20 SCHEMATIC OF MODELS SM 4 AND SM 5 SHOWING INTERACTION OF UIS WITH CORE STRUCTURE

free of the core ring. This amount of translation would also be required for the prototypical head, SM 8. The static test profiles of Figures 16 and 17 indicate that the UIS also delays disengagement of the LRP and IRP by restraining the relative rotation.

The static tests SM 7 and SM 8, the dynamic test SM 5, and the SDOF analysis employed to assist interpretation of test SM 5 and to predict the effect of replacing the head with one more prototypic have combined to point out the importance of including the UIS in any future head response analysis. The UIS is important because it provides a substantial restoring moment that limits deflections to safe values, certainly for the SM 7 head and probably for the SM 8 head. An analysis should be applied to verify the influence of the UIS on the SM 8 head during a dynamic test.

IV SUMMARY AND CONCLUSIONS

The two static tests of models of the CRBR head provided useful qualitative and quantitative data on the effects of shielding on the response of the head to HCDA loading. The primary differences in the two models centered on the design and attachment of the shielding to the three-plug models of the head. On model SM 7, the shielding and method of attachment were the same as that used on dynamic test SM 5; that is, the spacers between layers of shielding were machined into the shielding plates, and the plates were tightly fastened to the head with several strong bolts. The shielding on SM 8 was more prototypic. It included separate, thin spacer rings between shield layers and no bolt attachment of the shield plates to the head.

The following points summarize the important observations and conclusions drawn from the results of these two static tests.

- The bolts and integrally machined spacer rings on shield plates of model SM 7 strengthened the head. The head with more prototypic shielding (SM 8) had a stiffness that was 33% lower than the head with bolted shielding (SM 7).

- The head fails as a result of disengagement of the shear ring between the large and intermediate plugs. This failure is a gradual process that starts at a point along the shear ring interface nearest the center of the head at a displacement of 125 to 130 mils. Disengagement continues until the head can no longer carry a load. The displacement at failure is 250 mils. For SM 7, the failure load was 2587 psi, and for SM 8, the failure load was 2010 psi.

- Load-deflection and load-volume change records for both tests are mostly linear up to a displacement of about 50 mils (1500 psi) on SM 7 and of about 65 mils (1100 psi) on SM 8. At these displacements, the head begins to deform plastically.

- Data indicate that shielding "lockup" does not occur because shield plates can slide and realign themselves when contact is made between adjacent plates.

- An equivalent SDOF analysis that is based on an asymmetric model of the CRBR head with bolted shielding (SM 7) and with nonuniform mass distribution and a bilinear force-deflection relationship predicts a peak dynamic displacement of 89 mils under HCDA slug impact loading. This displacement is about 50% higher than the displacement measured on test SM 5 (~60 mils). A comparison of an SDOF analysis and a linear elastic finite element analysis of a three-piece plate indicates that the SDOF overpredicts peak displacement by about 16%. This degree of conservatism does not explain the difference between the SDOF predictions and the measurements on SM 5.

- The comparable SDOF analysis for the head with more prototypic shielding design and attachment (SM 8) predicts a peak displacement of 110 mils under HCDA slug impact loading. This displacement is 24% larger than that predicted for the head with bolted shielding.

- An explanation for the difference between the measured displacement on SM 5 and the predicted displacement using the SDOF technique is the restraining influence of the UIS on the rotation and displacement of the IRP to which the UIS is attached. Because the UIS is keyed into the core barrel and requires 225 mils of upward translation for disengagement from the barrel, the UIS cannot displace laterally. This constraint forces the UIS columns to apply a moment to the IRP as it tries to rotate during upward displacement.

- Results of the static tests SM 7 and SM 8, the dynamic test SM 5, and the SDOF analysis point out the importance of the UIS in limiting head deflections. As demonstrated by test SM 5, the UIS ensures a safe dynamic response of the SM 7 head and probably would ensure a safe response of the SM 8 head because it would remain engaged in the core barrel.

- Any future analyses should include the UIS.

Appendix A

TEST RESULTS

The load-deflection records for 16 out of 17 locations (Figure A.1) on each of the two heads tested on this program are shown in Figures A.2 through A.17. Records for location 17 are not shown because deflections at this location are less than one mil.

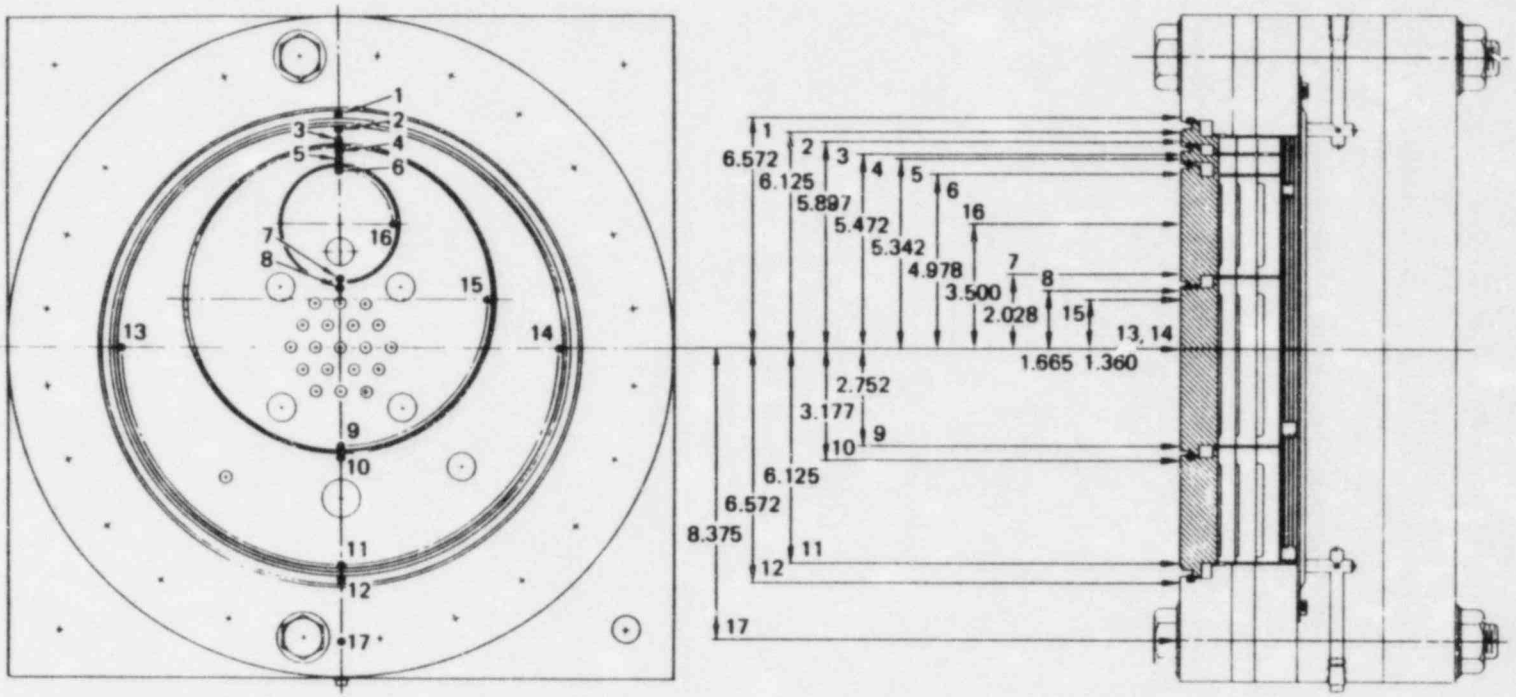

FIGURE A.1 INSTRUMENTATION LAYOUT FOR TESTS SM 7 AND SM 8

SM 7

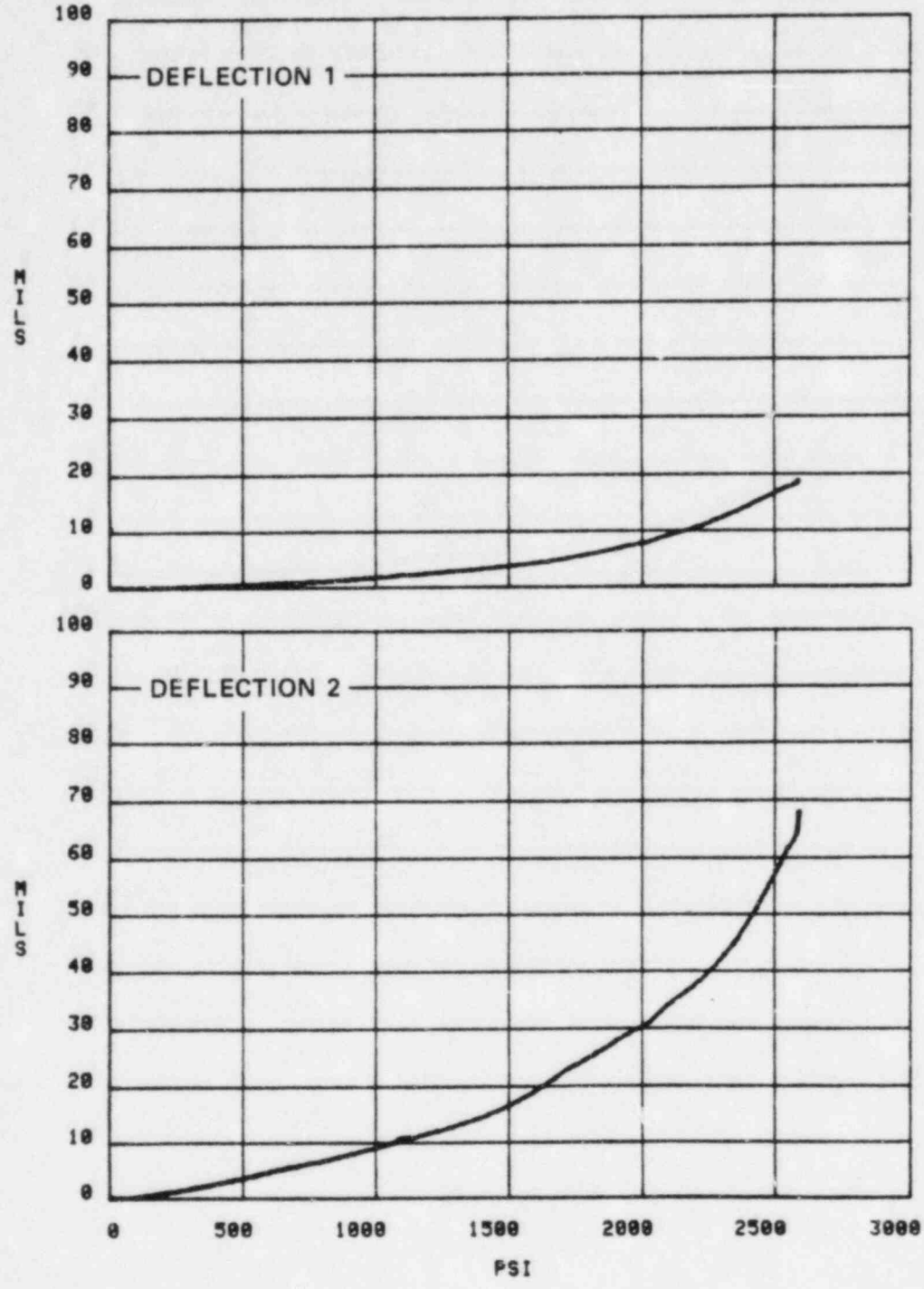

FIGURE A.2 DEFLECTION VERSUS PRESSURE FOR SM 7 GAGES 1 AND 2

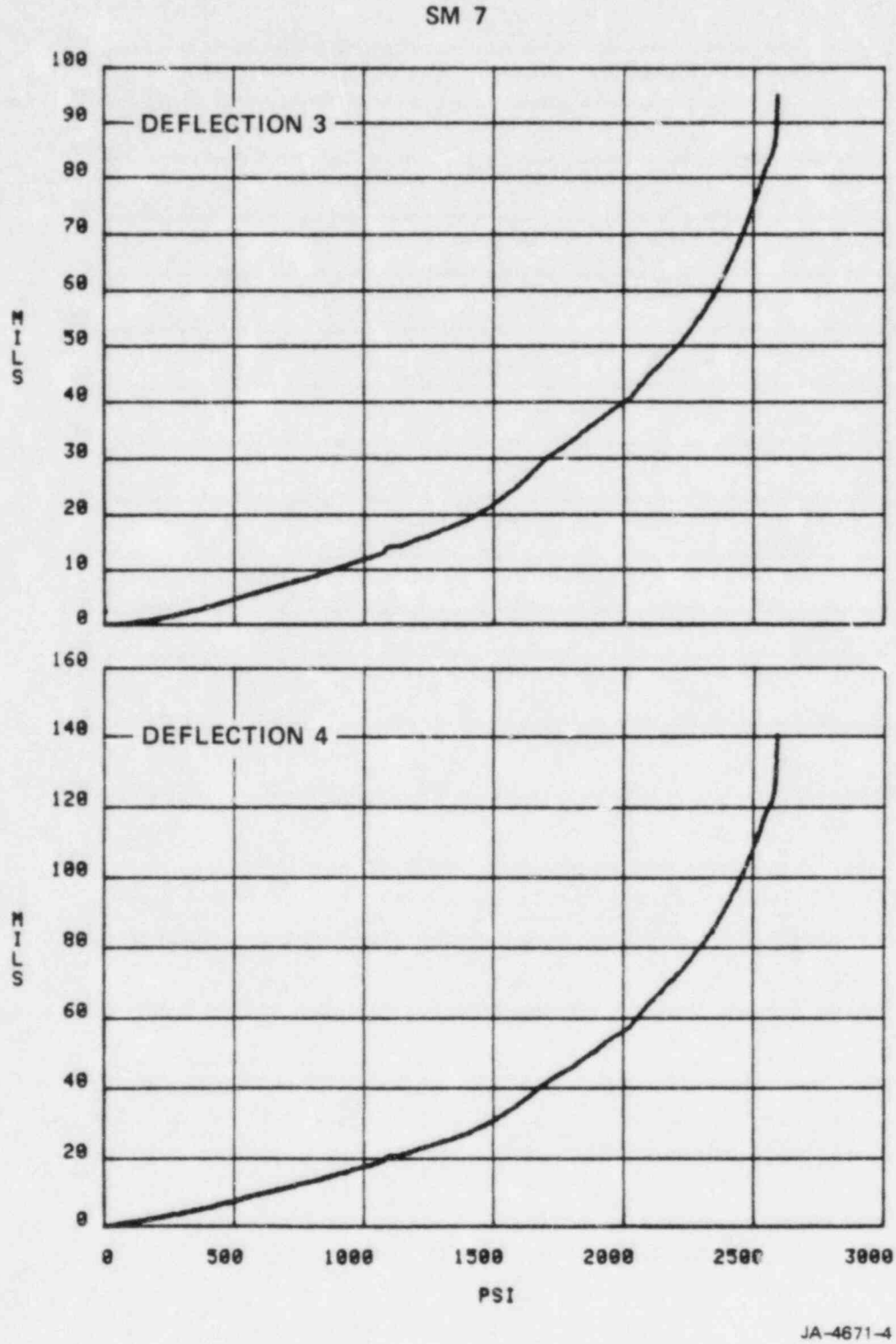

FIGURE A.3 DEFLECTION VERSUS PRESSURE FOR SM 7 GAGES 3 AND 4

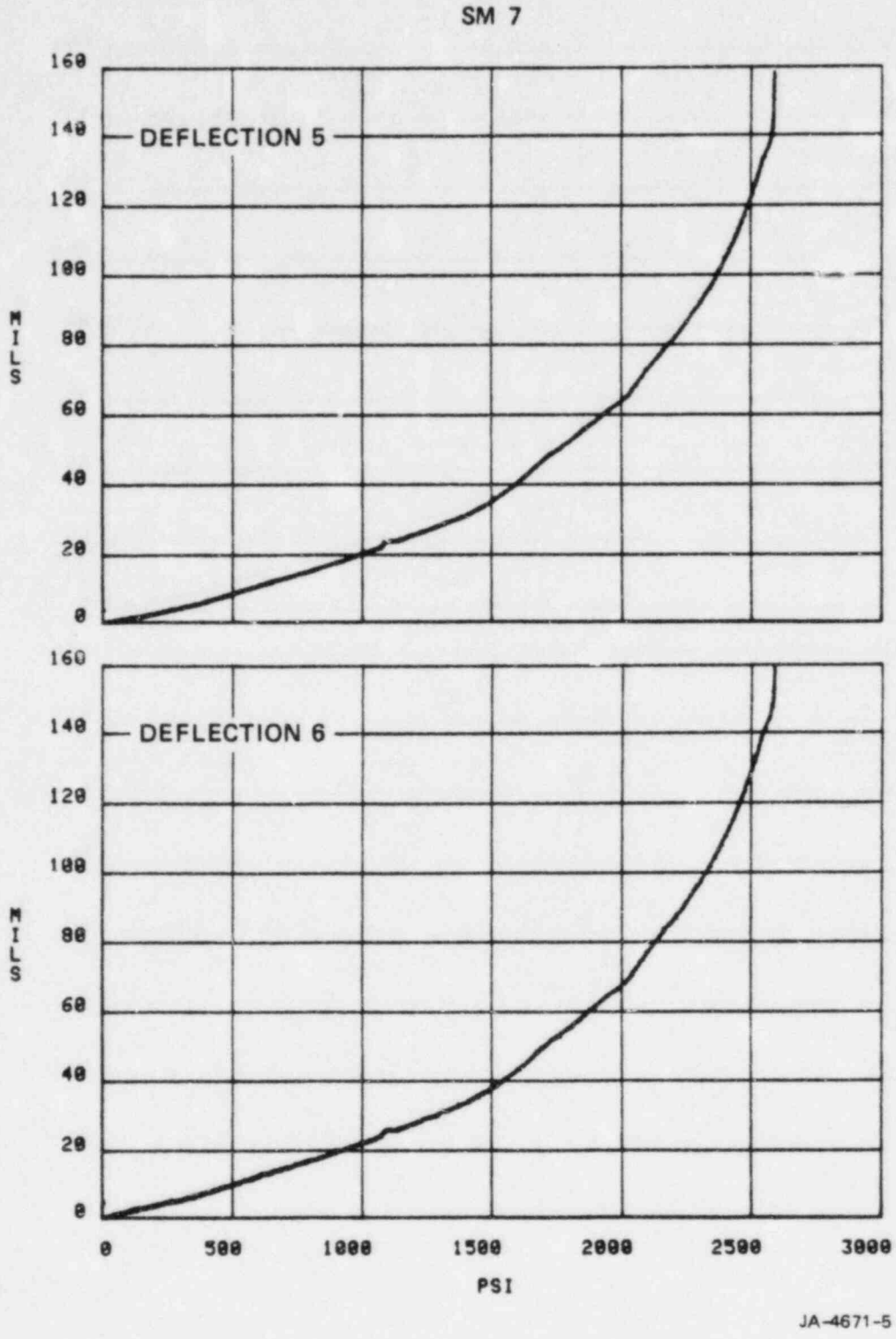

FIGURE A.4 DEFLECTION VERSUS PRESSURE FOR SM 7 GAGES 5 AND 6

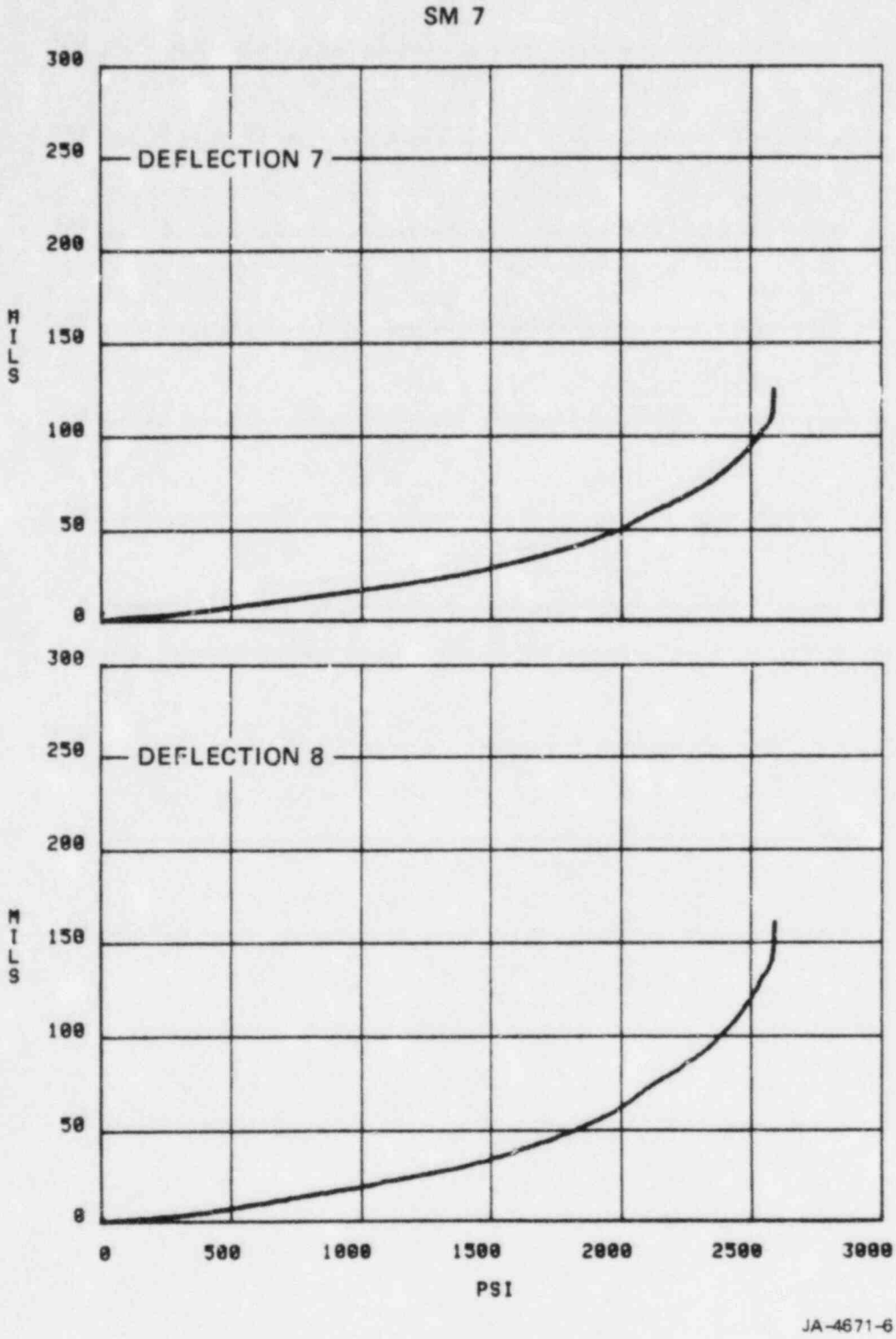

FIGURE A.5 DEFLECTION VERSUS PRESSURE FOR SM 7 GAGES 7 AND 8

SM 7

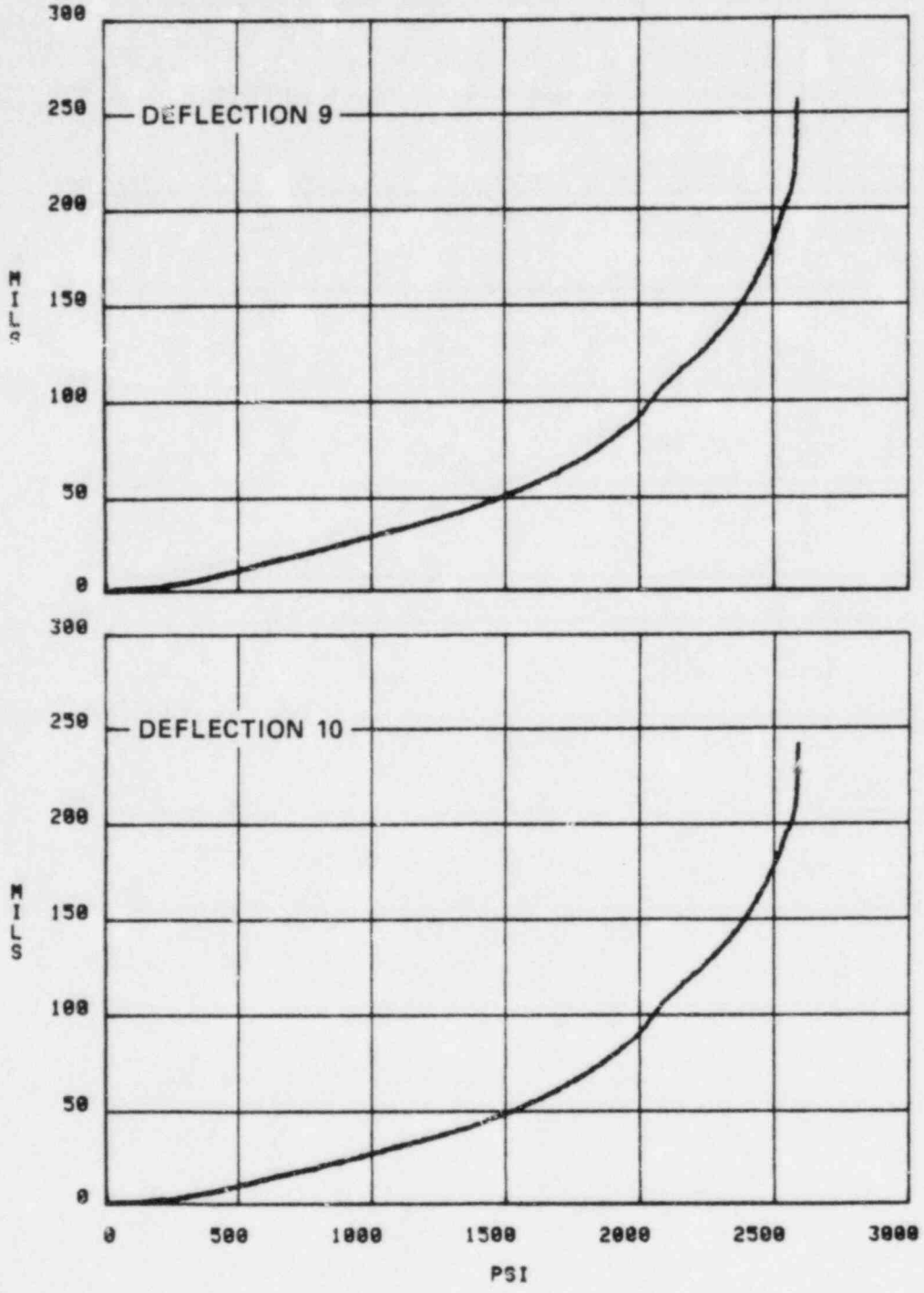

FIGURE A.6 DEFLECTION VERSUS PRESSURE FOR SM 7 GAGES 9 AND 10

SM 7

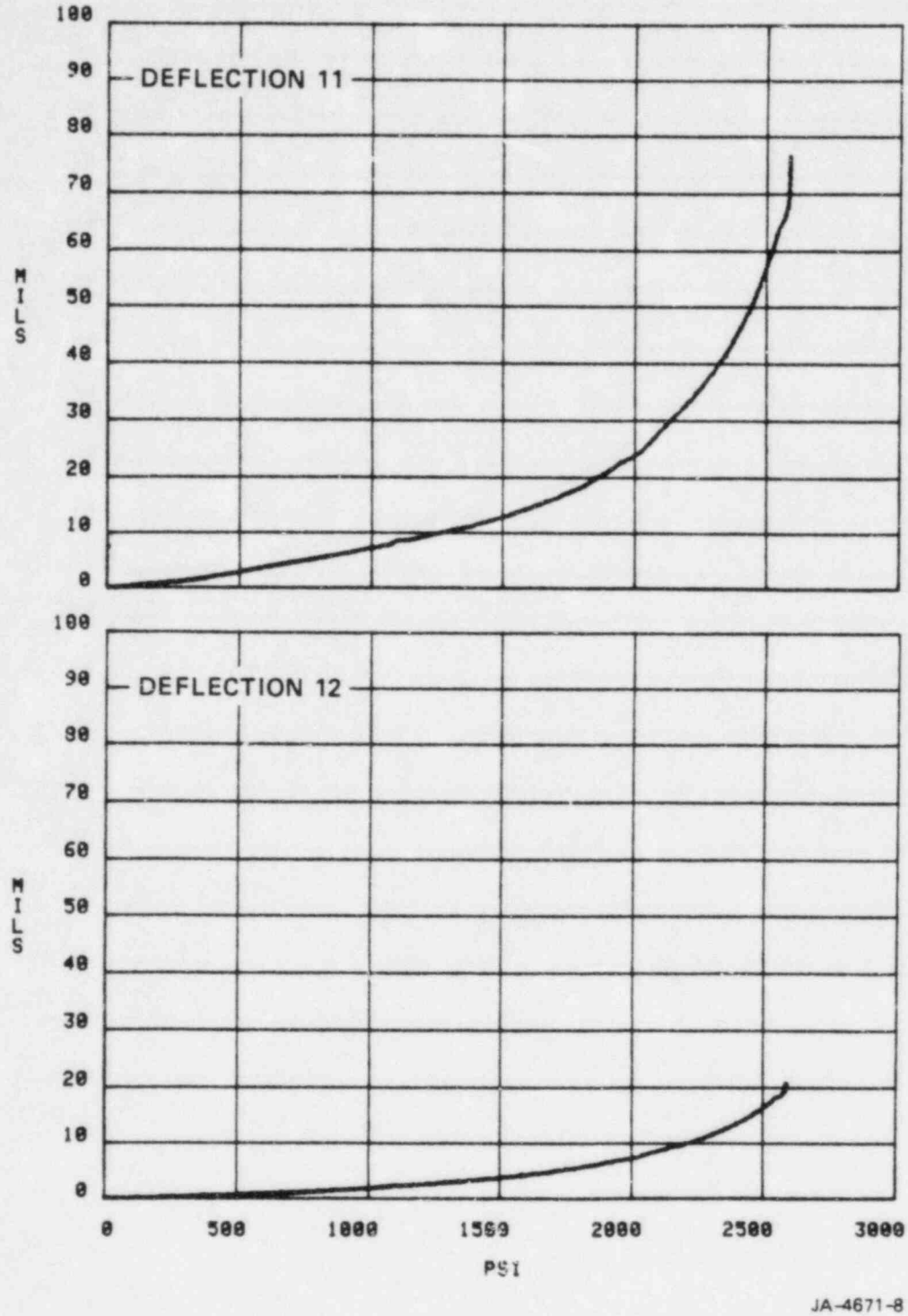

FIGURE A.7 DEFLECTION VERSUS PRESSURE FOR SM 7 GAGES 11 AND 12

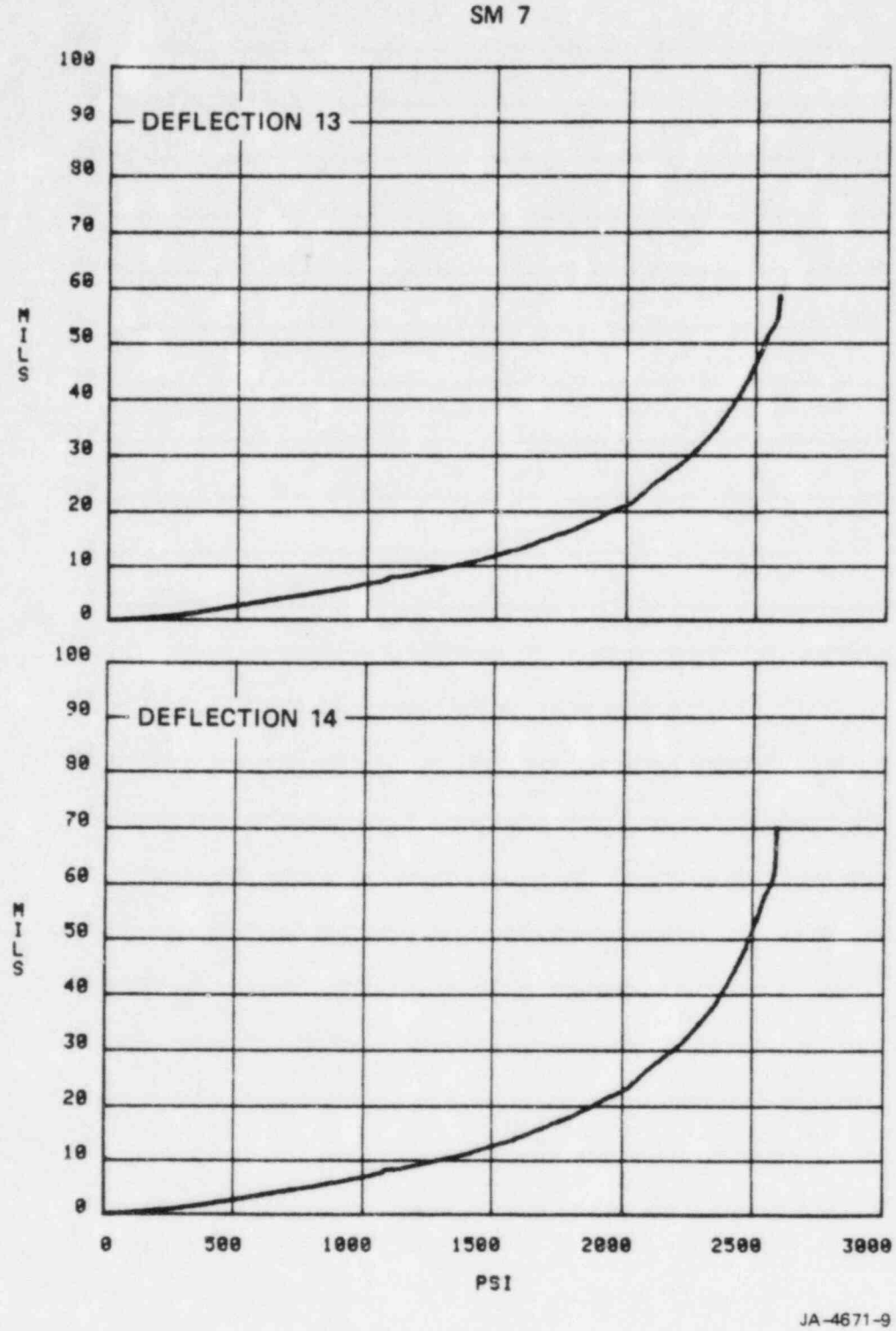

FIGURE A.8 DEFLECTION VERSUS PRESSURE FOR SM 7 GAGES 13 AND 14

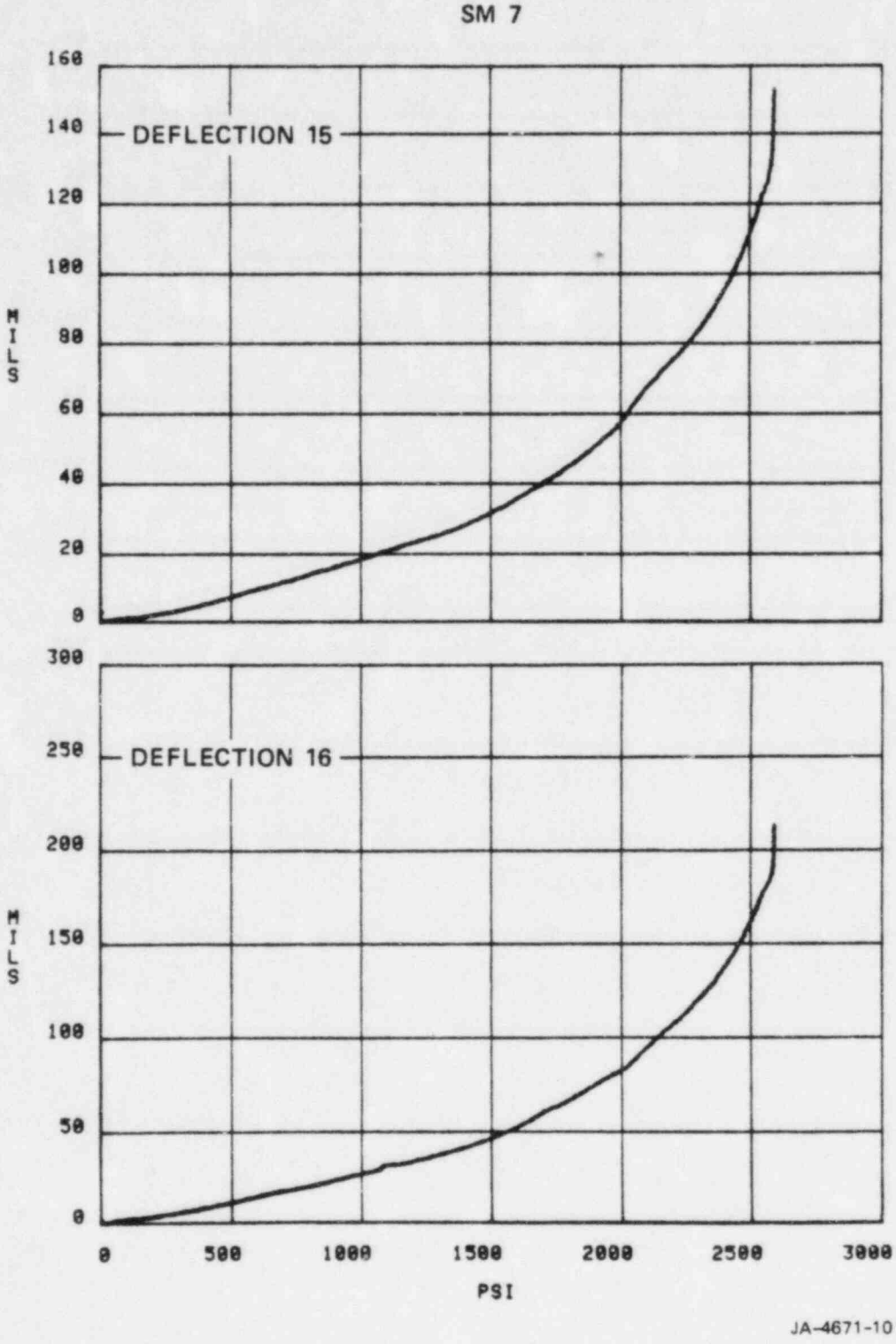

FIGURE A.9 DEFLECTION VERSUS PRESSURE FOR SM 7 GAGES 15 AND 16

SM 8

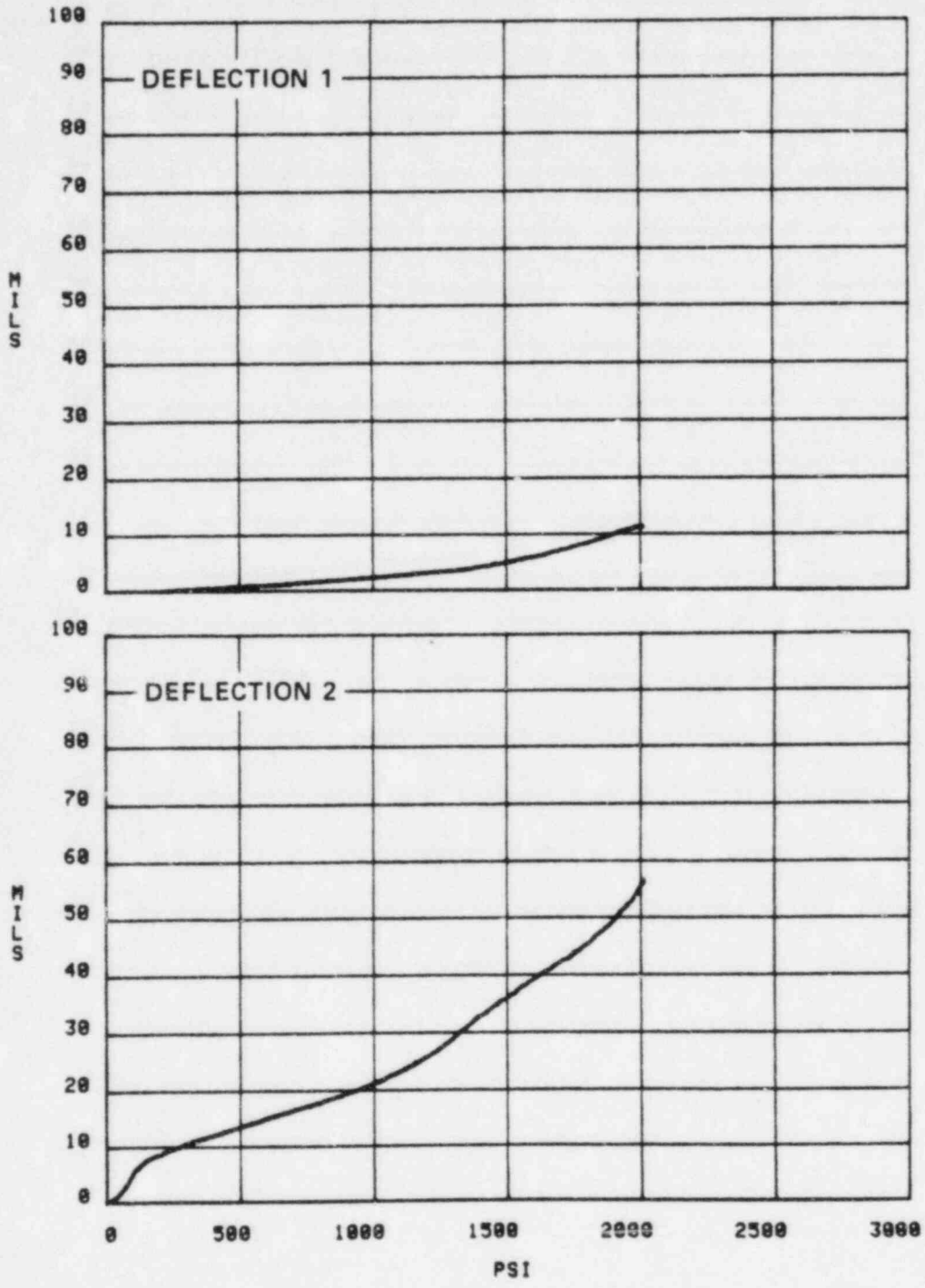

FIGURE A.10 DEFLECTION VERSUS PRESSURE FOR SM 8 GAGES 1 AND 2

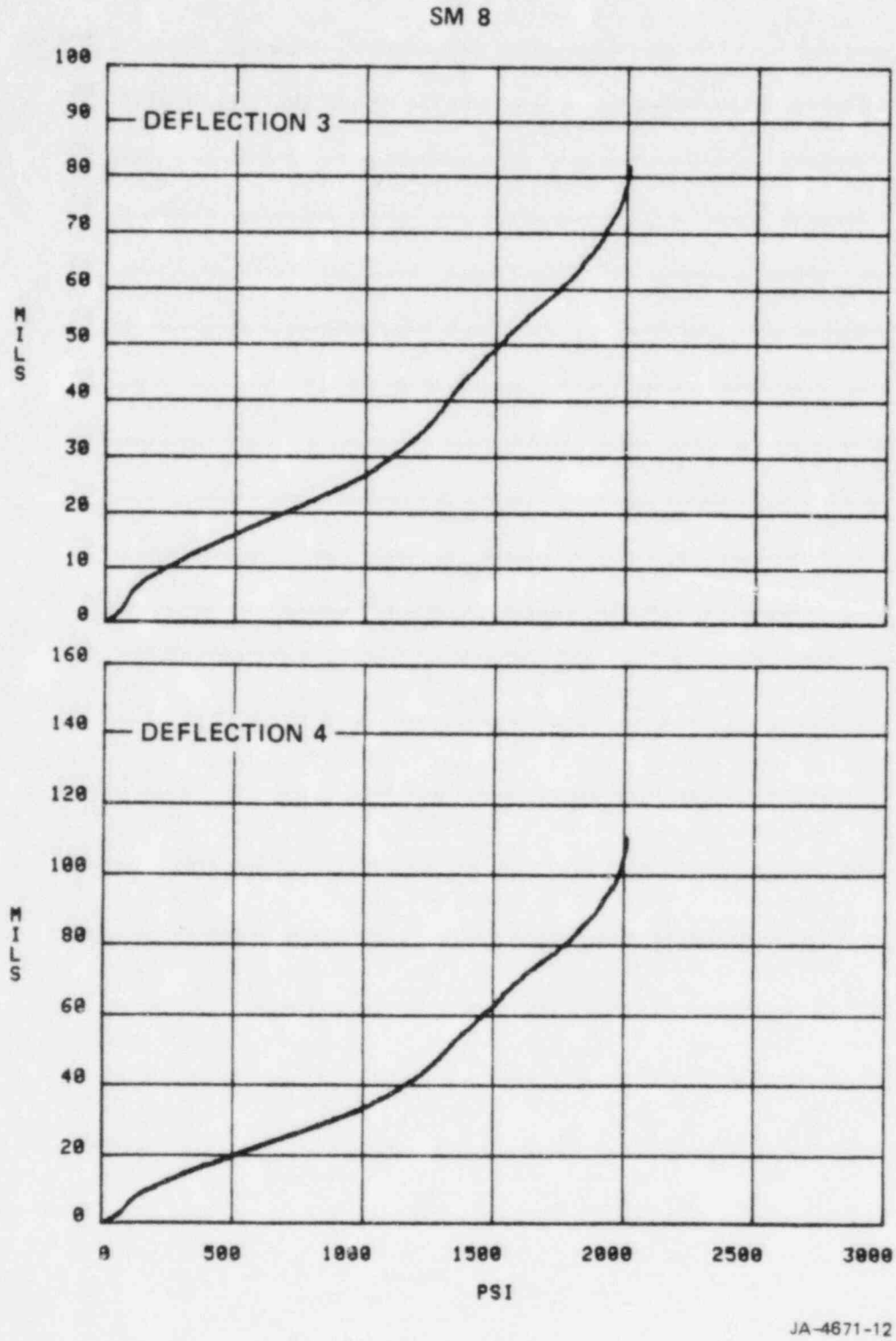

FIGURE A.11 DEFLECTION VERSUS PRESSURE FOR SM 8 GAGES 3 AND 4

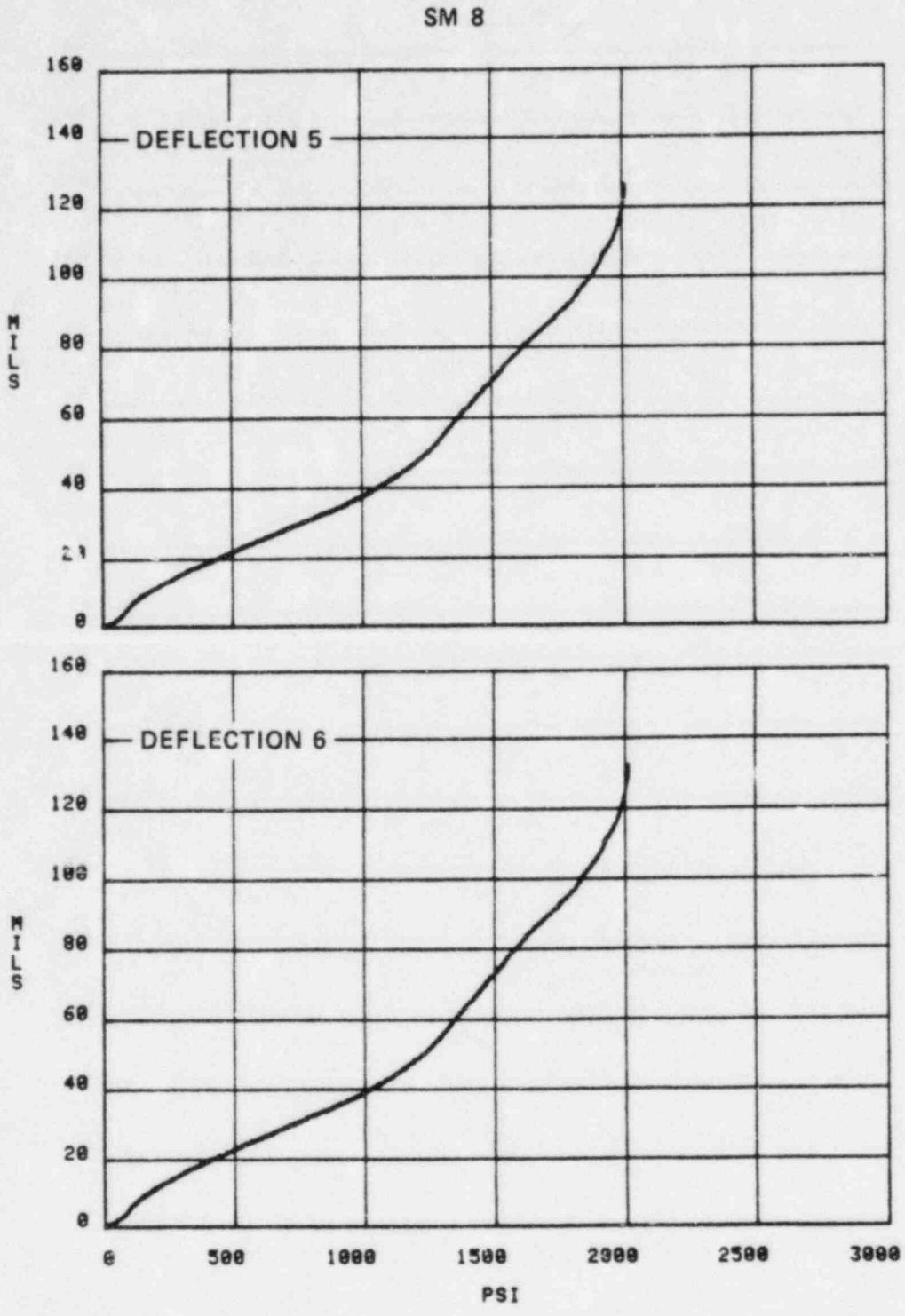

FIGURE A.12 DEFLECTION VERSUS PRESSURE FOR SM 8 GAGES 5 AND 6

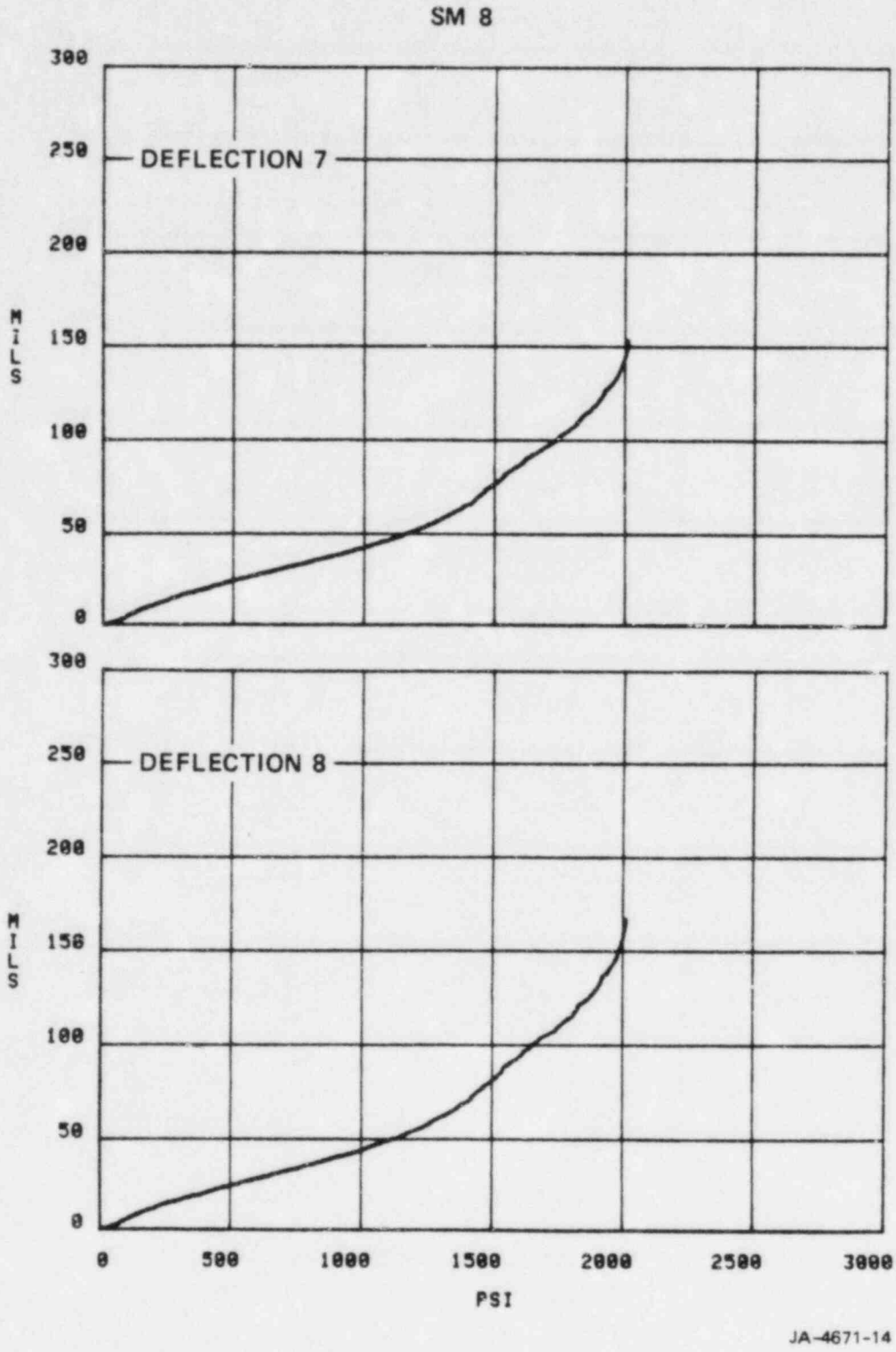

FIGURE A.13 DEFLECTION VERSUS PRESSURE FOR SM 8 GAGES 7 AND 8

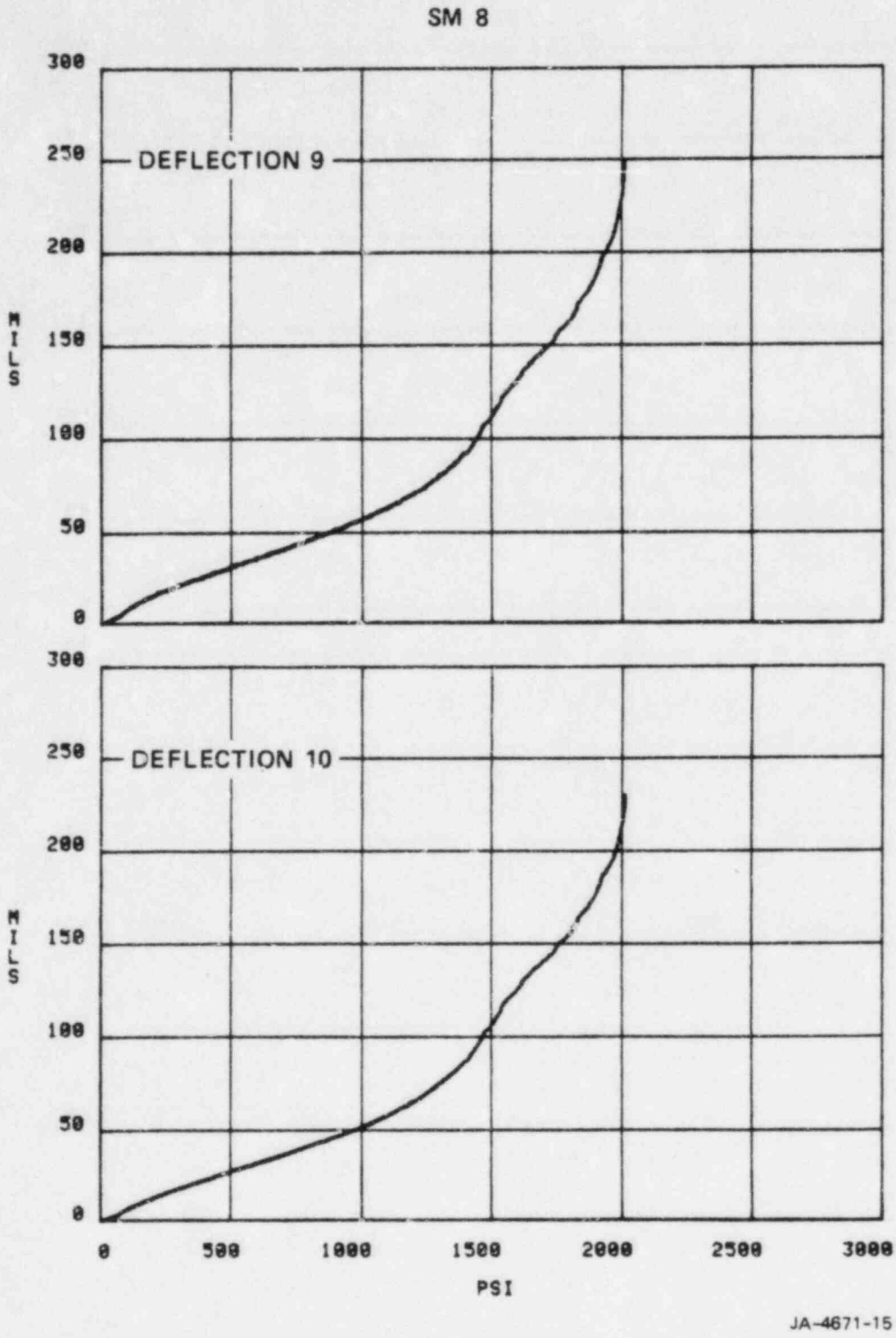

FIGURE A.14 DEFLECTION VERSUS PRESSURE FOR SM 8 GAGES 9 AND 10

SM 8

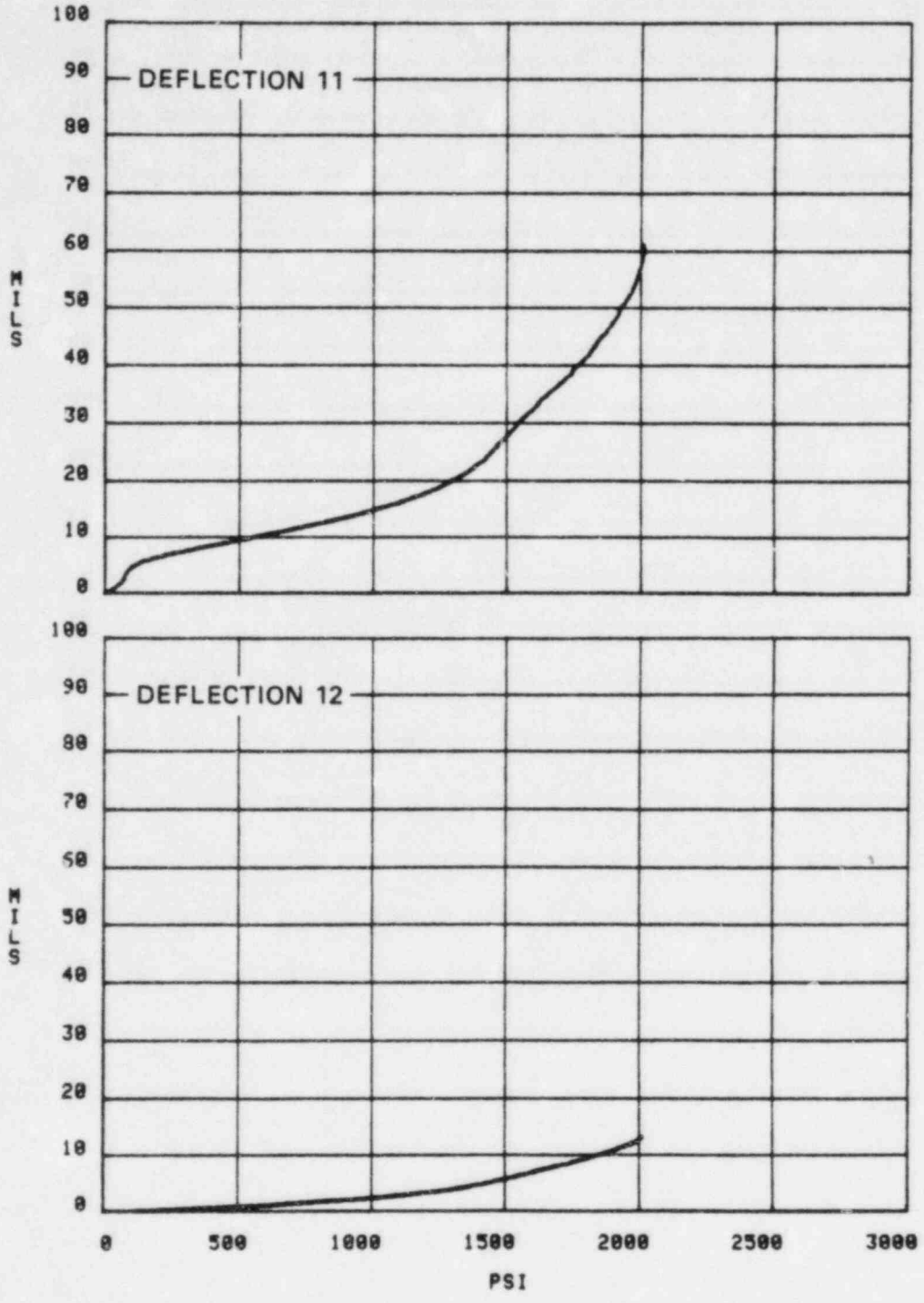

FIGURE A.15 DEFLECTION VERSUS PRESSURE FOR SM 8 GAGES 11 AND 12

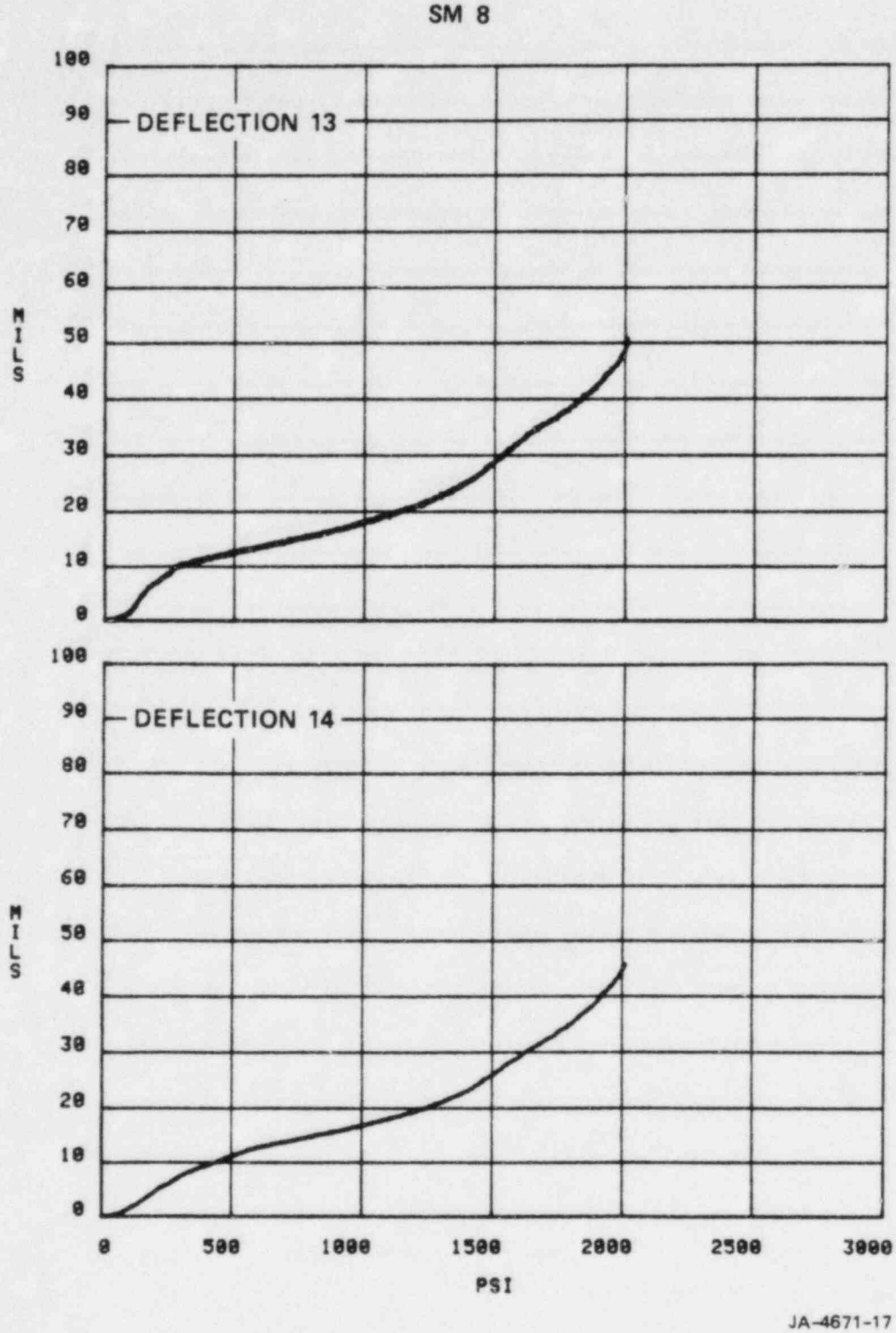

FIGURE A.16 DEFLECTION VERSUS PRESSURE FOR SM 8 GAGES 13 AND 14

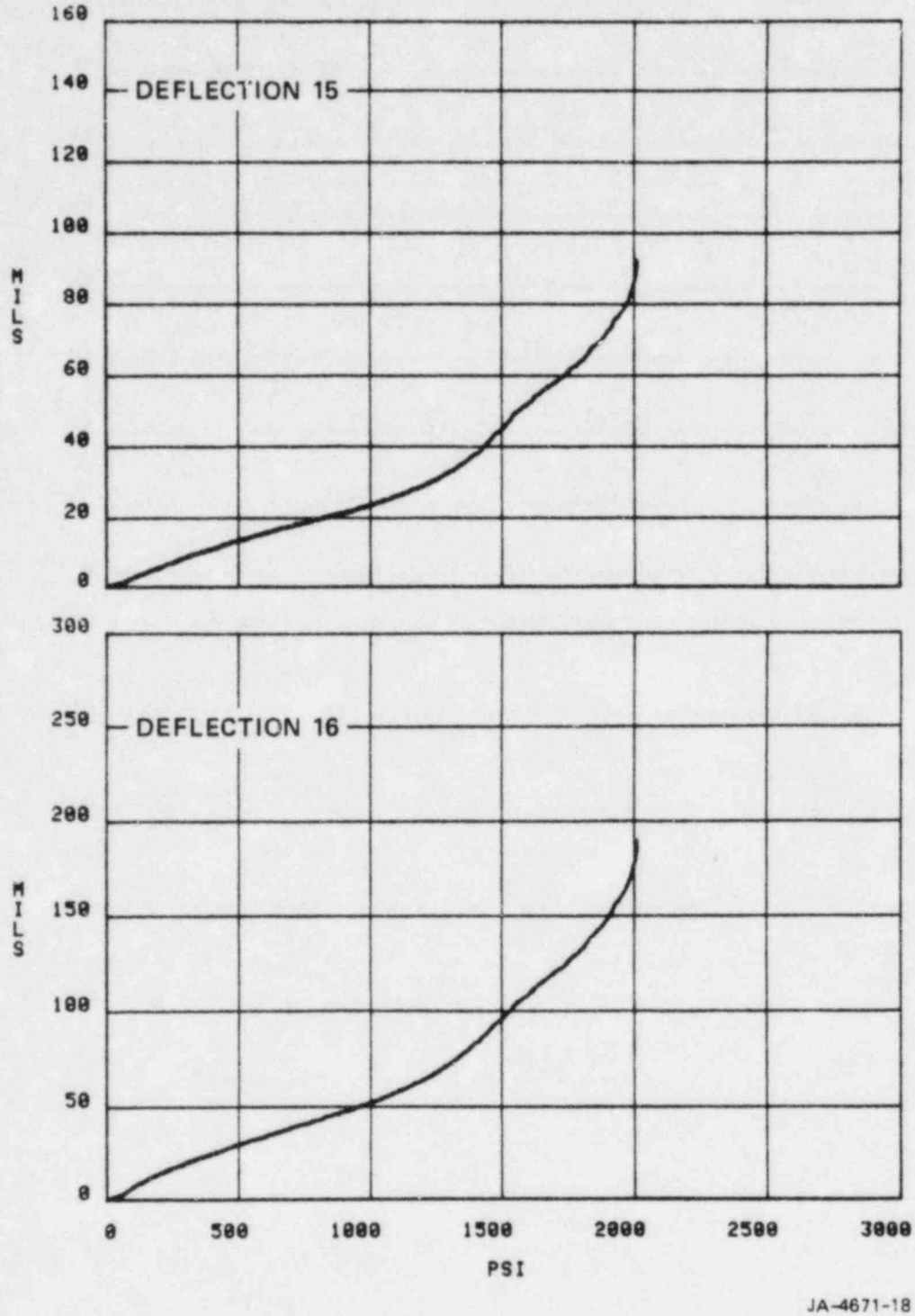

FIGURE A.17 DEFLECTION VERSUS PRESSURE FOR SM 8 GAGES 15 AND 16

Appendix B

DYNAMIC RESPONSE ANALYSIS OF THE CRBR HEAD

A. Objectives

The objective of this analysis is to evaluate the dynamic response of the CRBR head and shielding to the slug impact loading of a 661 MW-s HCDA. Three sets of dynamic response calculations are presented based on stiffness data gathered from static tests SM 1, SM 7 , and SM 8. In test SM 1, the stiffness of the head without shielding was obtained. This stiffness is added to the calculated stiffness of the shielding to estimate the combined stiffness of the head with shielding of the prototypic model. This combined stiffness was used to evaluate the response of the CRBR head in the dynamic test SM 5. In the second set of calculations, the stiffness obtained in Test SM 7 for the head with the shielding design of model SM 5 was used to predict the dynamic response of the head. Then, this prediction was compared with the SM 5 dynamic test results to provide a more realistic evaluation of test SM 5. In the third set of calculations, the stiffness obtained in Test SM 8 was used to predict the dynamic response of the head with more prototypic shielding.

B. Approach

The analytical approach is to develop a model of the head with the same pressure-volume relation as that experimentally determined for the asymmetric three-piece head. This model is then reduced to an equivalent single-degree-of-freedom (SDOF) system. The maximum deflection of the CRBR head caused by the slug impact loading of an HCDA is predicted by calculating the dynamic response of the SDOF system.

C. Single-Degree-of-Freedom Analysis

The response of the CRBR head to impulsive loading can be estimated by idealizing the three-piece symmetric or asymmetric model into an equivalent SDOF system. The equation of motion of the SDOF system is

$$M_e \ddot{X} + K_e X = F_e(t) \tag{B-1}$$

where M_e, K_e, and F_e are the effective mass, stiffness, and forcing function of the SDOF system, respectively. In the interest of conservatism, no damping has been included. M_e, K_e, and F_e of equation (B-1) are related to the mass M, stiffness K, and forcing function F of the real system by $M_e = K_m M$, $F_e = K_L F$, and $K_e = K_L K$. The constants are calculated once a deflection mode of the head is assumed. If the mode shape is $\phi(r,\theta)$, then the effective mass is

$$M_e = \int_A m\, \phi^2(r,\theta)\, dA \tag{B-2}$$

where m is the mass per unit area of the structure and A is the area of the structure being idealized. The effective forcing function is

$$F_e(t) = \int_A P(r,\theta,t)\phi(r,\theta)\, dA \tag{B-3}$$

where $P(r,\theta,t)$ is the pressure distribution and history. When P and m are assumed to be constant over the surface of the CRBR head model, constants K_m and K_L reduce to:

$$K_m = \frac{2}{a^2} \int_o^a \phi^2(r)\, r\, dr \tag{B-4}$$

$$K_L = \frac{2}{a^2} \int_o^a \phi(r)\, r\, dr \tag{B-5}$$

The first mode shape considered was the normalized deformed shape of the symmetric model of the head under the static pressure load. This mode shape is piecewise linear between hinge circles and is represented by:

$$\phi(r) = \begin{cases} 0.82\left(\frac{a - r}{a - b}\right) & b \leq r \leq a \\ 0.18\left(\frac{b - r}{b - c}\right) + 0.82 & c \leq r < b \\ 1.00 & 0 \leq r < c \end{cases} \qquad \text{(B-6)}$$

Substitution of the relationships (B-6) into (B-4) and (B-5) results in the SDOF constants $K_m = 0.497$ and $K_L = 0.629$.

A second mode shape was considered that is more characteristic of the deflected shape of the head. This asymmetric mode shape is simply the normalized static deflection of the heads of SM 7 and SM 8 at a load of 800 psi (Figures 16 and 17). The resulting SDOF constants are $K_m = 0.397$, $K_L = 0.593$, and $K = 2.7 \times 10^4$ psi/in. for SM 7 and $K_m = 0.460$, $K_L = 0.645$, and $K = 2.0 \times 10^4$ psi/in. for SM 8.

The forcing function that approximates the slug impact load is shown in Figure B.1. It is characterized by an initial impulse of magnitude $I_o = 0.38$ psi-s. This impulse is followed by a triangular load history corresponding to an initial pressure $P_o = 1200$ psi, which decays to zero in time $t_d = 1.2$ ms. The forcing function was idealized from loading pressures measured on the head during dynamic tests SM 4 and SM 5. The forcing function is expressed as

$$F(t) = I_o A_s \delta(t) + F_o(1 - t/t_d) \qquad \text{(B-7)}$$

where $F_o = P_o A_s$. The loaded area of the shielding is $A_s = 114$ in.^{2}. The Dirac-delta function, $\delta(t)$, is given by

$$\delta(t) = 0 \qquad t \neq 0$$

$$\int_{-\infty}^{\infty} \delta(t)dt = 1$$

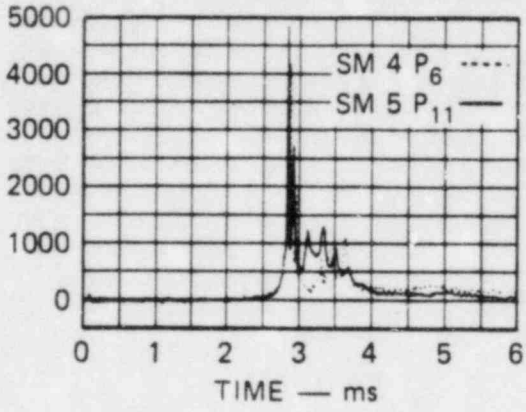

SLUG IMPACT LOAD

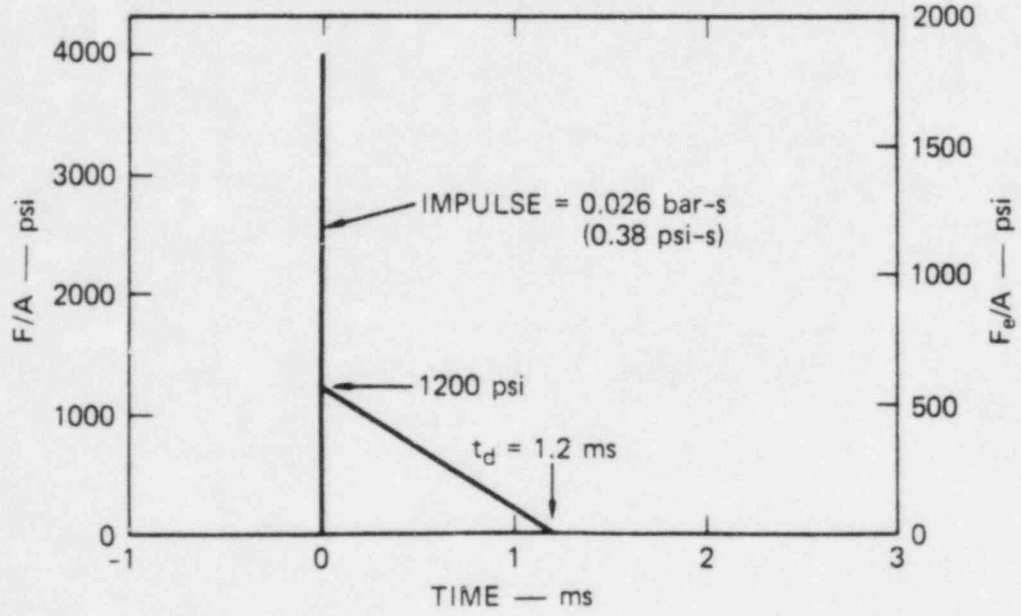

APPROXIMATION TO SLUG IMPACT LOAD

MA-3929-386

FIGURE B.1 EQUIVALENT SLUG IMPACT LOAD

The initial conditions of the SDOF system are usually $X(0) = 0$ and $\dot{X}(0) = 0$. However, the impulse $I_o A_s \delta(t)$ produces an instantaneous change in velocity. Integrating (B-1) over a short time interval Δt and taking the limit as $\Delta t \to 0$ results in the instantaneous change in velocity

$$\dot{X}(0) = \frac{I_o A_s K_L}{M K_m} \tag{B-8}$$

Using (B-8) as the initial velocity condition and the triangular load history of (B-7) as the forcing function, the equation of motion (B-1) is solved for the displacement and velocity histories

$$X(t) = \frac{\dot{X}(0)}{\omega} \sin \omega t + \frac{F_{oe}}{K_e} (1 - \cos \omega t) + \frac{F_{oe}}{K_e t_d} \left(\frac{\sin \omega t}{\omega} - t\right) \tag{B-9}$$

$$\dot{X}(t) = \dot{X}(0) \cos \omega t + \omega \frac{F_{oe}}{K_e} \sin \omega t + \frac{F_{oe}}{K_e t_d} (\cos \omega t - 1) \tag{B-10}$$

where $\omega = (K_e/M_e)^{1/2}$ and $F_{oe} = K_L F_o$. Setting $\dot{X}(t) = 0$ determines the time t_{max} when the maximum deflection occurs. Substituting t_{max} into (B-9) determines the maximum deflection X_{max}.

The natural period of vibration of the SDOF system is:

$$T_e = 2\pi \sqrt{\frac{M_e}{K_e}} \tag{B-11}$$

The effective stiffness of the SDOF system is calculated from

$$K_e = K_L A \frac{P}{W_{max}} \tag{B-12}$$

D. Stiffness Properties of the CRBR Head with Shielding

Calculations were performed in a gradual process of model refinement and for assessing the effects on head deflection of parameters such as stiffness, mass distribution, and interplate friction. The model variations were divided into the following categories:

- A symmetric model in which the head has the same linear elastic stiffness as SM 1. Symmetric shield plates are added theoretically to produce a combined stiffness so no interplate friction is included. The mass is uniform.

- An asymmetric model in which the head has the same linear elastic stiffness as SM 1. Asymmetric shield plates are added theoretically to produce a combined stiffness so no interplate friction is included. The mass is nonuniform.

- A symmetric model in which the combined stiffness is the same as the linear elastic portion of the SM 7 stiffness curve. The mass is uniform.

- An asymmetric model in which the combined stiffness is the same as the linear elastic portion of the SM 7 stiffness curve. The mass is uniform. Variations consist of a nonuniform mass, a bilinear stiffness to account for the initial pressure-volume slope, and a trilinear stiffness to also include approximately a final pressure-volume slope.

- A symmetric model in which the combined stiffness is the same as the linear elastic portion of the SM 8 stiffness curve. The mass is uniform.

- An asymmetric model in which the combined stiffness is the same as the linear elastic portion of the SM 8 stiffness curve. The mass is uniform. Variations consist of a nonuniform mass, a bilinear stiffness to account for the initial pressure-volume slope, and a trilinear stiffness to also include approximately a final pressure-volume slope.

Our first set of calculations was performed with the three-piece symmetrical model of the CRBR head shown in Figure B.2. The outer diameters of the plugs in the symmetric model and asymmetric head are equal. The shear rings are approximated by circular hinges. The loads

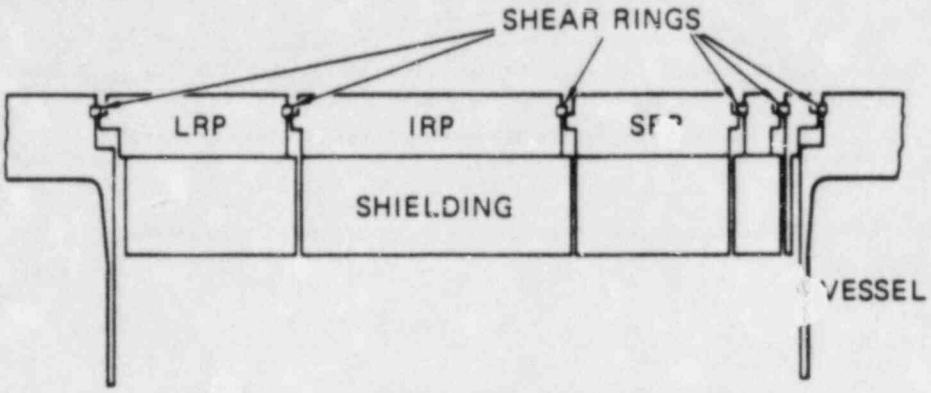

THREE-PIECE CRBR HEAD WITH SHIELDING

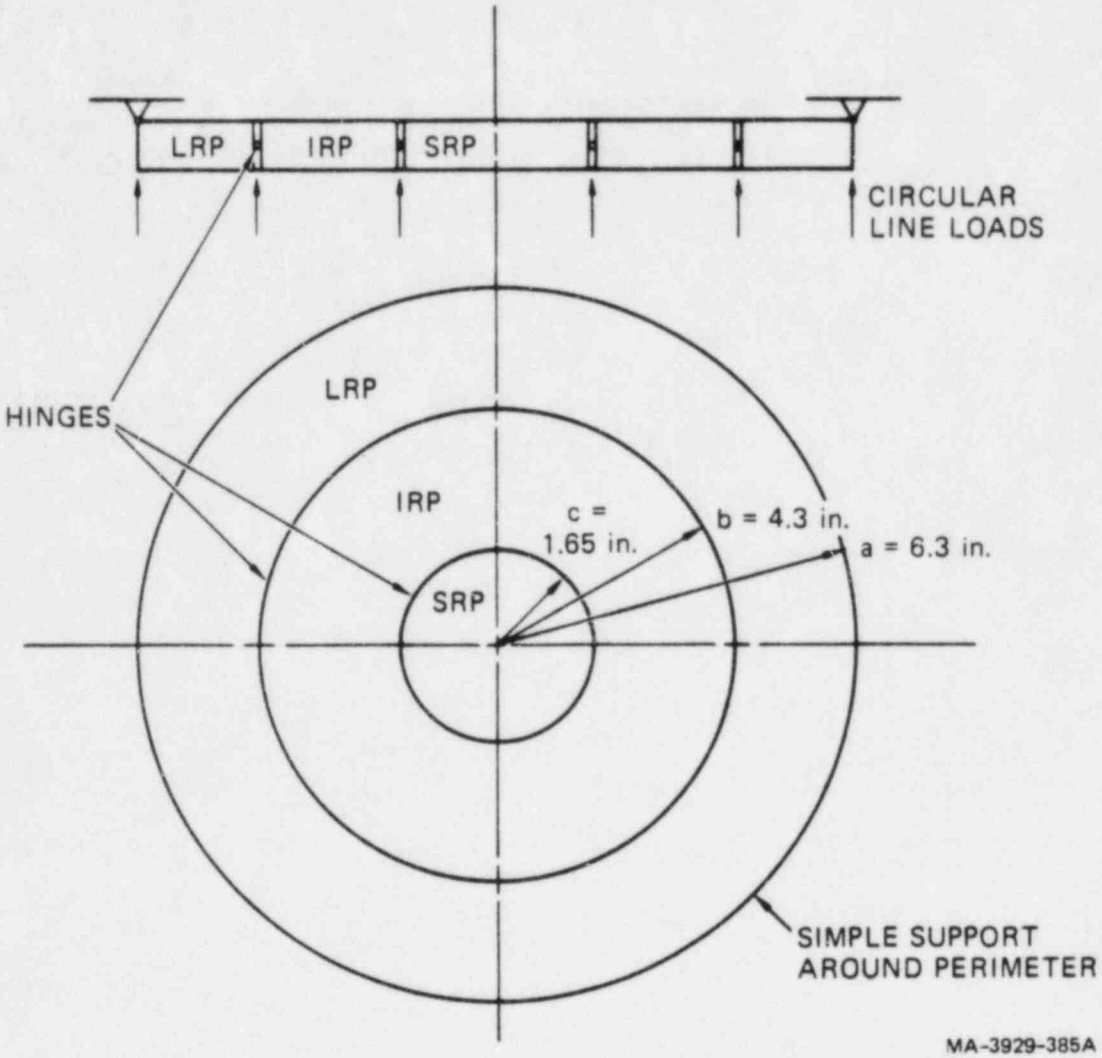

FIGURE B.2 SYMMETRICAL MODEL OF CRBR HEAD

applied to each plug were approximated by circular line loads applied at the hinges. The circular line loads at the hinges include the resultant pressure applied uniformly to the next smaller plug and the distributed pressure resultant pushing up on the annular plate. This distribution is required because the shielding does not make contact over the entire surface of each annular plate but rather along its inner and outer perimeter. The flexural rigidity of the composite plate is the sum of the flexural rigidities of the head and three layers of shielding individually.

The calculated pressure-volume relation of the three-piece symmetric head is

$$V = 15235 \frac{P}{D_h + 3D_s} \qquad \text{(B-13)}$$

where P is the applied pressure in psi, V is the volume under the domed head in $in.^3$, and D_h and D_s are the flexural rigidities in lb-in. of the head and one layer of shielding, respectively. The volume under the head is determined by first calculating the deflections of each annulus at hinge locations b and c. The deformed shape of each annulus is then assumed to be a conical frustum that deflects linearly from one hinge to the next. The SRP is displaced as a rigid body but does not deform.

In the elastic range of the SM 1 experimental data, the slope of the pressure-volume record (Figure B.3) is $P/V = 130$ psi/$in.^3$. When this slope is substituted into (B-2) with $D_s = 0$, the flexural rigidity of the three piece symmetric head is $D_h = 2.0 \times 10^6$ lb-in. For steel, this is equivalent to a plate thickness of 0.90 inch. If the thickness of each layer of the steel shielding is 0.5 inch, then $3D_s = 1.0 \times 10^6$ lb-in. The combined flexural rigidity of the head with shielding is 3.0×10^6 lb-in.

The calculated pressure deflection relation of the symmetric head with shielding is

$$W_{max} = \frac{194\ P}{D_h + 3\ D_s} \qquad \text{(B-14)}$$

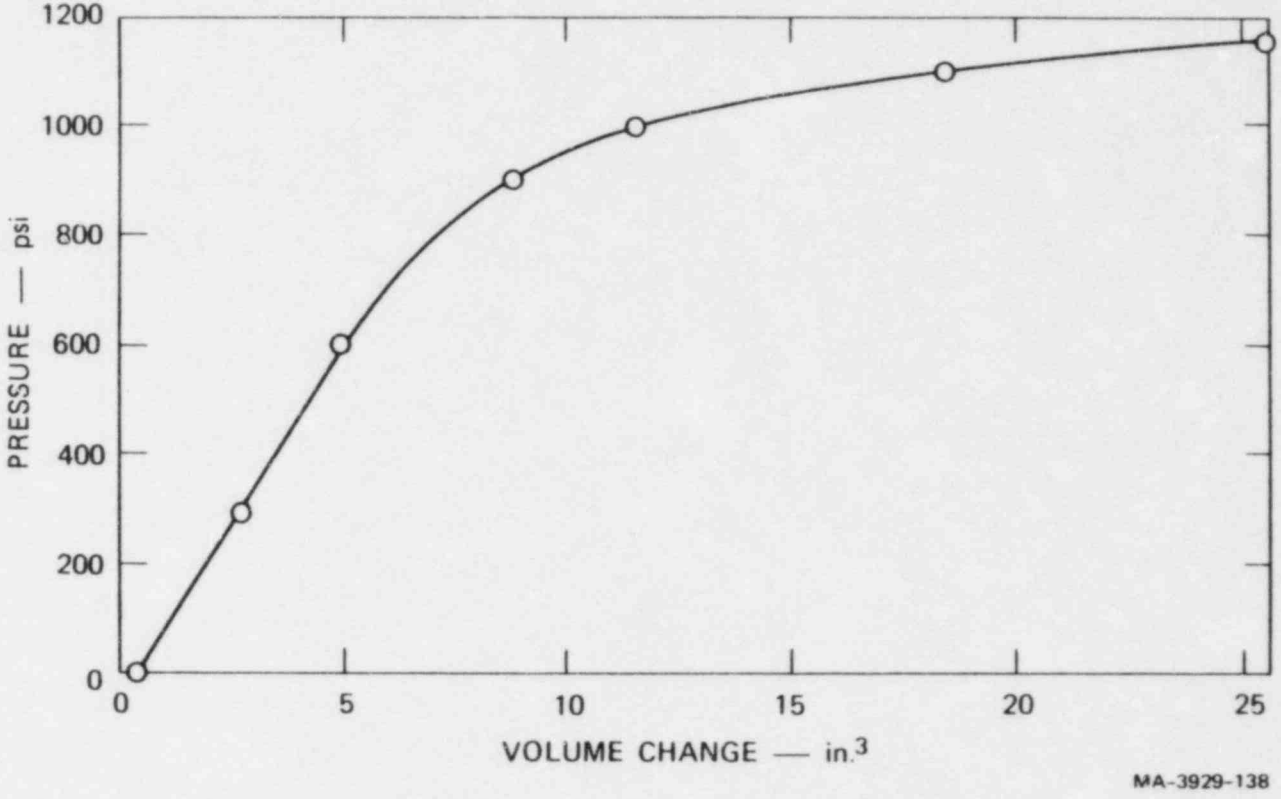

FIGURE B.3 PRESSURE-VOLUME CHANGE RELATION FOR SM 1

where W_{max} is the maximum deflection of the head in inches. Using D_h = 2.0×10^6 lb-in. in (B-1) and setting $D_s = 0$, the slope of the pressure-deflection curve for the head without shielding is $P/W_{max} = 1.02 \times 10^4$ psi/in. In the elastic range of the SM 1 experimental data, the pressure-deflection slope of the LRP near the LRP-IRP shear ring location is approximately 1.0×10^4 psi/in. This is in good agreement with the calculated slope indicating that by equating the volumes under the symmetric model and asymmetric head, the maximum deflections are also matched.

The data from Test SM 1 were also used to estimate the stiffness of the asymmetric three-piece prototypical head by adding the flexural rigidities of the asymmetric shield plates as calculated from theoretical results supplied by the Advanced Reactor Division of the Westinghouse Electric Corporation.* Among the results supplied, those concerning the bottom, middle, and top LRP shields were used. The shield plates were simply supported around the outer circle and hinged around the inner circle. They were deformed by a vertical force applied to a rigid circular plug that fitted inside the hole. The linear elastic relationship between the force and the maximum deflection was provided for each LRP shield plate. The stiffnesses in this form were 157, 164, and 119 lb/mil for the bottom, middle, and top LRP shield plates, respectively. From these values the combined stiffnesses in the form required were found to be $P/W_{max} = 0.5 \times 10^4$ psi/in. (combined flexural rigidity $D = 1.0 \times 10^6$ lb-in.). Hence the stiffness of the head with shielding is $P/W_{max} = 1.5 \times 10^4$ psi/in. ($D = 3.0 \times 10^6$ lb-in.). The corresponding pressure-volume relationship, assuming the SM 8 mode shape, is $P/V = 187$ psi/in.^{3}.

Table B.1 lists the stiffness properties of the CRBR head based on static tests SM 1, SM 7, and SM 8. The pressure-volume ratios for SM 7 and SM 8 were calculated from the central linear portions of the

---

*Letter reference number WL820667, December 23, 1982. (Attachment 3)

SM 7 and SM 8 pressure-volume records shown in Figure B.4. Using these slopes in (B-13) with $D_h + 3D_s$ replaced by D, the combined flexural rigidity of the head with shielding, D, is calculated. This flexural rigidity is then substituted into (B-14) to determine the head stiffness P/W_{max}. The stiffness can also be determined from the pressure-deflection record for gage 9 at the LRP-IRP junction. For SM 7, the measured stiffness is approximately 2.7×10^4 psi/in. which is 8% lower than the symmetric model stiffness. For SM 8, the measured stiffness is approximately 2.0×10^4 psi/in., which is in agreement with the calculated stiffness.

Table B.1

STIFFNESS PROPERTIES OF THE CRBR HEAD MODELS

Model	P/V (psi/in.^{3})	P/W_{max} (psi/in.)	D (lb-in.)
SM1 (Sym. shields)[a]	197	1.55×10^4	3.0×10^6
(asym. shields)[a]	187	1.50×10^4	3.0×10^6
SM7	372	2.92×10^4	5.67×10^6
SM8	251	1.97×10^4	3.82×10^6

[a]These models represent zero friction cases.

E. SDOF Maximum Deflection Predictions

Table B.2 presents the results of the dynamic analysis based on static tests SM 1, SM 7, and SM 8. These results indicate that the asymmetric model predicts slightly larger peak displacements than the symmetric model (see last column). However, because the real head is asymmetric, the asymmetric model results should be used.

A further refinement of the SDOF analysis is to use a more realistic distribution of mass on the asymmetric head. The masses of the LRP,

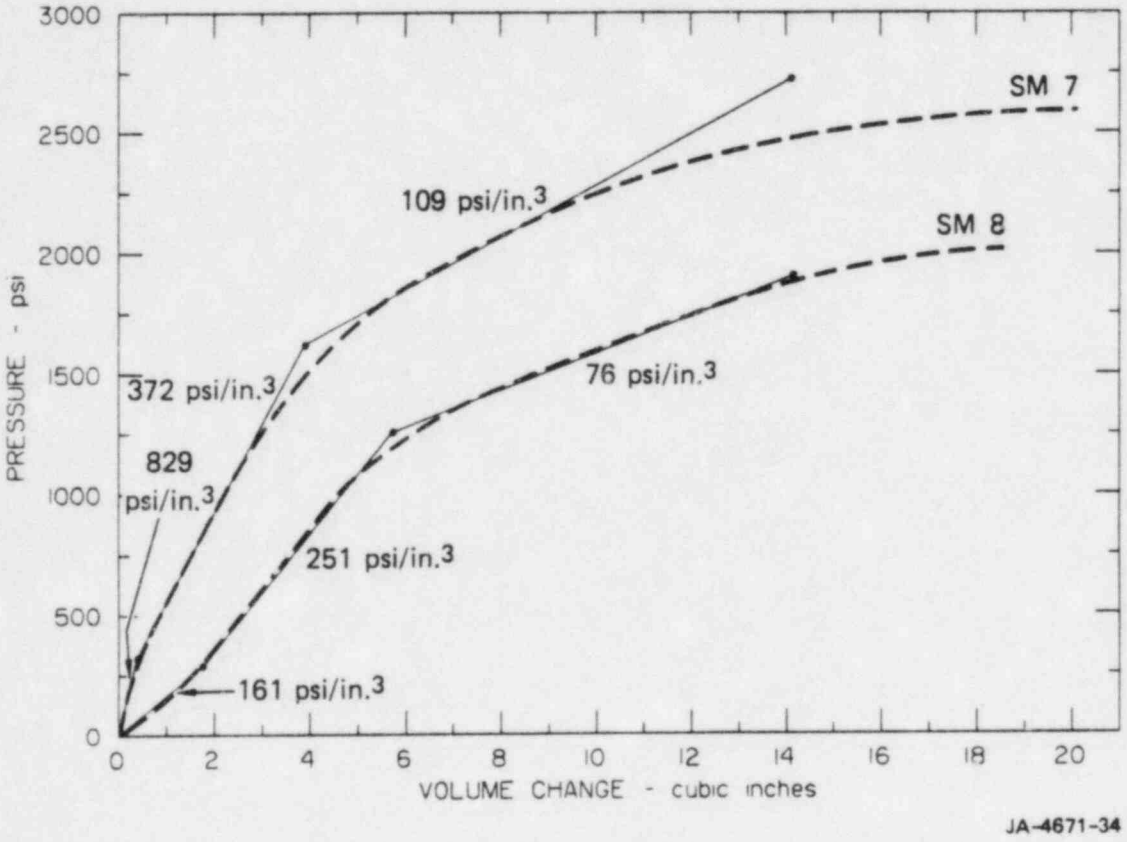

FIGURE B.4 PRESSURE-VOLUME CHANGE RELATIONS FOR SM 7 AND SM 8

Table B.2

SDOF PROPERTIES AND PREDICTED MAXIMUM HEAD DEFLECTIONS

Model	Mode Shape	M_e (lb-s^2/in.)	K_e (lb/in.)	F_{oe} (lb)	T_e (ms)	$\dot{X}(0)$ (in./s)	t_{max} (ms)	X_{max} (in.)
SM 1	Sym[a]	0.178	1.21×10^6	8.62×10^4	2.41	152	0.80	0.129
SM 7	Sym	0.178	2.30×10^6	8.62×10^4	1.75	152	0.58	0.082
SM 8	Sym	0.178	1.55×10^6	8.62×10^4	2.13	152	0.70	0.109
SM 7	Asym	0.142	2.00×10^6	8.12×10^4	1.67	199	0.55	0.091
SM 8	Asym	0.165	1.61×10^6	8.84×10^4	2.01	168	0.66	0.111
SM 1	Asym, non-uniform mass[a]	0.177	1.21×10^6	8.84×10^4	2.41	157	0.80	0.133
SM 7	Asym, non-uniform mass	0.153	2.00×10^6	8.12×10^4	1.74	166	0.57	0.089
SM 8	Asym, non-uniform mass	0.177	1.61×10^6	8.84×10^4	2.08	157	0.69	0.109
SM 7	Asym, non-uniform mass, bilinear force-deflection	0.153	4.45×10^6 2.00×10^6	8.12×10^4	--	166	0.57	0.089
SM 8	Asym, non-uniform mass, bilinear force-deflection	0.177	1.03×10^6 1.61×10^6	8.84×10^4	--	157	0.69	0.110
SM 7	Asym, non-uniform mass, trilinear force-deflection	0.153	4.45×10^6 2.00×10^6 0.59×10^6	8.12×10^4	--	166	1.06	0.179
SM 8	Asym, non-uniform mass, trilinear force-deflection	0.177	1.03×10^6 1.61×10^6 0.49×10^6	8.84×10^4	--	157	1.20	0.202

[a]These models represent zero friction cases.

IRP, and SRP are 25.15 kg, 28.57 kg, and 3.54 kg, respectively. The distributed mass is assumed to be constant for each plug. Using these masses along with the asymmetric mode shape increases the equivalent mass constants to $K_m = 0.427$ for SM 7 and $K_m = 0.494$ for SM 8. The dynamic effect is a small reduction in peak deflections to 0.089 inch for SM 7 and 0.109 inch for SM 8.

Another refinement of the SDOF analysis is to use a bilinear stiffness curve to include the initial loading behavior (Figure B.4). For SM 7 the bilinear pressure-volume relationship selected was:

$$P/V = \begin{cases} 829 \text{ psi/in.}^3 & 0 \leq V \leq 0.391 \text{ in.}^3 \\ 372 \text{ psi/in.}^3 & 0.391 \text{ in.}^3 < V \end{cases}$$

The peak dynamic deflection of SM 7 is reduced to 0.089 inch using the bilinear stiffness curve. For SM 8 the bilinear pressure-volume curve was

$$P/V = \begin{cases} 161 \text{ psi/in.}^3 & 0 < V < 1.762 \text{ in.}^3 \\ 251 \text{ psi/in.}^3 & 1.762 \text{ in.}^3 < V \end{cases}$$

The peak dynamic deflection of SM 8 increases to 0.110 inch.

The final refinement to the SDOF analysis is to use a trilinear pressure-volume relationship. This trilinear curve accounts for the nonlinearity of the head response at low pressure and for the nonlinear response from plastic deformation and disengagement at high pressures. For SM 7, the trilinear pressure-volume curve is approximated by:

$$P/V = \begin{cases} 829 \text{ psi/in.}^3 & 0 \leq V \leq 0.391 \text{ in.}^3 \\ 372 \text{ psi/in.}^3 & 0.391 \text{ in.}^3 \leq V \leq 3.84 \text{ in.}^3 \\ 109 \text{ psi/in.}^3 & 3.84 \text{ in.}^3 < V \end{cases}$$

The peak dynamic deflection for SM 7 increases to 0.179 inch. For SM 8, the trilinear pressure-volume curve is approximated by:

$$P/V = \begin{cases} 161 \text{ psi/in.}^3 & 0 \leq V \leq 1.762 \text{ in.}^3 \\ 251 \text{ psi/in.}^3 & 1.762 \leq V \leq 5.65 \text{ in.}^3 \\ 76 \text{ psi/in.}^3 & 5.65 < V \end{cases}$$

The peak dynamic deflection for SM 8 increases to 0.202 inch.

F. SDOF Overprediction

An estimate of the overprediction was obtained by performing two linear elastic analyses on a symmetric, three-piece plate subjected to a triangular pulse load similar to that measured in Test SM 5. One analysis was performed with the finite element code WHAM and the other was performed with the SDOF technique. In this example, the maximum deflection predicted by the SDOF analysis was about 16% greater than that predicted by the finite element analysis. This percentage should serve as a reasonable estimate for the SDOF overprediction. However, as demonstrated below, another factor appears to have a much larger influence on the predictions.

G. Summary of Deflection Results

The principal results extracted from Table B.2 are listed in Table B.3

H. Comparison of Experimental and SDOF Results

In the static tests SM 7 and SM 8 plastic flow occurs when the deflection is about 60 mils, and disengagement of the LRP and IRP initiates when the deflection is about 130 mils. The SDOF analysis of SM 7 indicates that in the dynamic test SM 5 some plastic flow would occur and possibly even slight disengagement (see last two columns of Table B.3), even allowing for a crude 16% overprediction of the deflection. However, in the dynamic test SM 5 no measurable plastic strains were produced, and the maximum deflection was only 60 mils. Therefore, an important restraining mechanism was acting on the head. This

Table B.3

PREDICTED MAXIMUM DEFLECTIONS

Geometry	Mass	P/V	Deflection (mils) SM 1[a]	SM 7	SM 8
Sym.	--	--	129	82	109
Asym.	--	--	--	91	111
Asym.	Nonuniform	Linear	133	89	109
Asym.	Nonuniform	Bilinear	--	89	110
Asym.	Nonuniform	Trilinear	--	179	202

*Experimental stiffness of head and theoretical stiffness of shields (zero friction cases).

restraining mechanism was caused by the upper internal structure (UIS), which was locked into the head and the upper core barrel former ring (Figure 20). After the simulated HCDA event, the UIS was still locked into the head and core ring, and the main UIS deformation was caused by axial buckling. Thus, throughout the upward motion of the head a substantial restoring moment was applied to the IRP, thereby restricting upward deflections. Allowing for the observed UIS shortening of 170 mils, an upward IRP translation of 225 mils is required before the UIS can become free of the core ring. This amount of translation would also be required for the prototypical head, SM 8. The static test profiles of Figures 16 and 17 indicate that the UIS also delays disengagement of the LRP and IRP by restraining the relative rotation

I. Conclusion

Results of the static tests SM 7 and SM 8, the dynamic test SM 5, and the SDOF analysis used to assist interpretation of test SM 5 and to predict the effect of replacing the head with one more prototypic point

out the importance of including the UIS in any future head response analysis. The UIS is important because it provides a substantial restoring moment that limits deflections to safe values, certainly for the SM 7 head and probably for the SM 8 head. An analysis should be applied to verify the influence of the UIS on the SM 8 head during a dynamic test.